Selected Studies in Exobiology, Planetary Environments, and Problems Related to the Origin of Life

Semiannual Progress Report No. 1
for the period 1 October 1965
through 31 March 1966
Grant No. NGR-09-015-023

June 1966

Smithsonian Institution
Astrophysical Observatory
Cambridge, Massachusetts 02138

Selected Studies in Exobiology, Planetary Environments, and Problems Related to the Origin of Life

Semiannual Progress Report No. 1
for the period 1 October 1965
through 31 March 1966
Grant No. NGR-09-015-023

June 1966

Smithsonian Institution
Astrophysical Observatory
Cambridge, Massachusetts 02138

5-66-23

Selected Studies in Exobiology, Planetary Environments, and Problems Related to the Origin of Life

Principal Investigator - Dr. Carl Sagan

The initial 6 months of this grant were spent primarily in the development of column chromatographic and infrared spectrometric techniques and equipment for laboratory work, and the consideration of a variety of theoretical problems. A Perkin-Elmer Model 621 infrared spectrometer has been ordered and delivered. A range of accessories, including the 40-m long-path White cells, has yet to be delivered. Hiring an infrared spectroscopist has turned out to be more difficult than we had originally anticipated, but we are now in the final stages of negotiation with a widely experienced spectroscopist, and we anticipate that infrared experimentation will be in progress by the summer. Apparatus for column chromatography, including the fraction collector, has been assembled and will be in use by the summer in a continuation of our search for amino acid-nucleotide interactions. Three students will be employed on the grant by this summer.

In the first 6-month period of the grant, we have pursued a range of searches for amino acid-nucleotide interaction on paper chromatography, as well as a variety of experiments on the synthesis of amino acids from reducing gases using longer wave ultraviolet light than has been used in the past. Because of the exponential shape of the solar Planck distribution function toward short wavelengths, a successful production of amino acids by long-wave ultraviolet light would imply much larger rates of amino-acid synthesis on the primitive Earth than has been suspected heretofore.

On the theoretical side three papers have been completed: "An Analysis of the Mariner 2 Microwave Observations of Venus," submitted to the Astrophysical Journal; "Properties of the Clouds of Venus," in press, in Proceedings of the JPL - Caltech Lunar and Planetary Conference, Harrison Brown et al., editors, 1966; and "Thermodynamic Equilibria in Planetary Atmospheres," submitted to the Astrophysical Journal. A copy of each of these papers is enclosed at the end of this report.

Current theoretical problems that are now being written up include:

(1) Analysis of radar Doppler spectroscopy of Mars;

(2) A discussion of elevation differences and surface pressures on Mars;

(3) A new analysis of the photometric and polarimetric properties of the Martian surface;

(4) A new inorganic model of the Martian wave of darkening, and of associated seasonal and secular changes of the Martian surface;

(5) An analysis of the Mariner 4 photography of Mars; and

(6) A comprehensive analysis of the Venus greenhouse effect.

An infrared planetary camera developed with Smithsonian Institution internal funds has not been completed, and initial attempts at infrared planetary photography with the 61-inch Agassiz telescope of Harvard College Observatory will be made in the near future, supported in part with funds from this grant.

An Analysis of the Mariner 2 Microwave Observations of Venus

James B. Pollack
Smithsonian Astrophysical Observatory
Cambridge, Mass.

and

Carl Sagan
Harvard University
and
Smithsonian Astrophysical Observatory
Cambridge, Mass.

Received,

Smithsonian Institution
Astrophysical Observatory
Cambridge, Massachusetts 02138

ABSTRACT

The limb-darkening observations of Venus made by the 19-mm channel of the United States spacecraft Mariner 2 are here analyzed and compared with ground-based measurements in a hot-surface context. The peak brightness temperatures, T_{Bp}, near the center of each scan (dark side, terminator, bright side); the temperatures, $T(z_e)$, of the effective subsurface emitting level for 19-mm radiation; and the total optical depths, τ, of the overlying microwave attenuators are related by a simultaneous solution of the equations of radiative transfer and heat conduction, here performed for five different opacity models: pressure-induced transitions of CO_2 and N_2, continuously distributed throughout the atmosphere; nonresonant and resonant absorption by water vapor, similarly distributed; an aerosol of absorbing dust, arbitrarily distributed; an isothermal absorbing cloud layer, near the top of the atmosphere; and an aerosol of scattering particles, arbitrarily distributed with altitude. The temperature, $T(z_e)$, is derived from ground-based observations at longer wavelengths where $\tau = 0$ closely. Then τ(19 mm) is determined for the terminator scan, where all probable errors are smallest, and is found in good agreement with values deduced from recent measurements of the 8-mm phase effect. The peak brightness temperatures for the bright and dark sides are then derived to determine whether agreement with the Mariner 2 observations can be secured for any reasonable distribution of surface temperature and opacity. On this basis, the CO_2-N_2, the water vapor, and the absorbing dust models are rejected. The failure of the pressure-induced CO_2-N_2 transition model sets an upper bound on the Cytherean surface pressure in the 115-to-150 atm range, and demonstrates that pressure-induced transitions of CO_2 and N_2 are not the principal sources of millimeter opacity on Venus. Similarly, the failure of the water vapor model sets an upper bound on the total water vapor abundance: 85 g/cm^2 if the surface dielectric constant ϵ(19 mm) = 1.45 (as one interpretation of the 3.6-cm radar results suggests), and 45 g/cm^2 if ϵ(19 mm) = 3.6 (as radar results at longer wavelengths suggest).

The surviving isothermal cloud and distributed scatterer models point to sizable longitudinal temperature gradients, in quantitative agreement with gradients inferred from observations of the 3- and 10-cm phase effects. In these models, self-consistency between bright-side and dark-side scans are investigated for a variety of possible analytic forms of the surface temperature distribution. Consistency is achieved for the models in which clouds or scatterers are above an $\epsilon = 3.6$ surface only for a steep analytic form of the latitudinal gradient; for the cloud model with surface $\epsilon = 1.45$, a more modest gradient is required.

A possible discriminant among the successful models is the value of ϵ(19 mm), the surface dielectric constant for 19-mm emission; it is also approximately the value of ϵ deduced from 3.6-cm radar observations. If ϵ(19 mm) $\simeq 1.45$, then only the absorbing cloud model survives, and liquid water droplets as the primary opacity source are strongly indicated. If ϵ(19 mm) $\simeq 3.6$, then both absorbing and scattering models survive. In the scattering models the observed limb darkening is perhaps best realized by dust continuously distributed through the atmosphere; but hailstones or large raindrops are also possible. For all scattering models, particle radii very close to 0.5 mm are required. Such particles have terminal velocities of several tens of miles per hour.

I. INTRODUCTION

On 14 December 1962 the United States spacecraft Mariner 2 passed within 6 planetary radii of the surface of Venus. A two-channel microwave radiometer was aboard the spacecraft. This experiment was conceived (see Jones 1964, p. 116) in part to test a water model of the clouds of Venus proposed by Sagan and Giver (1961). During three scans--of the dark side, the terminator, and the bright side of the planet--the emissions at wavelengths 13.5 and 19 mm were recorded as a function of position on the disk. With the antenna polarization adopted, unambiguous limb darkening was observed in the 19-mm channel (Barath, Barrett, Copeland, Jones, and Lilley 1964). This result, together with other lines of evidence (Walker and Sagan 1966), renders the ionospheric model of the Cytherean microwave emission untenable, and suggests that the observed radiation arises from a hot surface and atmosphere (see, e.g., Sagan and Kellogg 1963). While other efforts have been made to circumvent the necessity for a hot surface (see, e.g., Tolbert and Straiton 1962; Scarf 1963), these have not been developed in any great detail, and no attempts have been made to account with them for a wide range of observations of Venus. On the other hand, the hypothesis of a hot surface can account in a perfectly self-consistent way for the details of the near infrared rotational temperatures (Spinrad 1962a; Sagan 1962), of the passive interferometric microwave observations (Pollack and Sagan 1965a; henceforth called "Paper I"; Clark and Kuz'min 1965), and of the microwave phase effect (Pollack and Sagan 1965b; henceforth called "Paper II"). In the present paper we undertake to study the consistency of the hot-surface model in explaining the observed limb darkening at millimeter wavelengths as well.

At wavelengths shorter than 3 cm, the brightness temperature of Venus declines rather markedly, a phenomenon generally attributed to a sharp increase in the atmospheric opacity. Suggested sources of this attenuation include gaseous constituents of the atmosphere, particularly CO_2 and N_2 mixtures, and H_2O (Barrett 1961; Thaddeus 1965; Barrett and Staelin 1964); atmospheric dust (Öpik 1961); and clouds composed of water (Sagan and Giver 1961; Rasool 1963; Salomonovich 1964; Diermendjian 1964). In the present paper we will determine the extent to which each of these attenuators can explain the Mariner 2 limb-darkening observations. In so doing we will gain some knowledge, in the context of the hot-surface model, of the nature of the millimeter attenuator and of the distribution of surface temperature over the Cytherean surface.

Previous theoretical studies designed to discriminate among the various postulated sources of opacity have been made by Barrett and Staelin (1964), and by Pollack and Sagan (Paper II). Barrett and Staelin have compared the observed functional dependence of brightness temperature on wavelength with the spectrum predicted by each of the putative attenuators. It was found that each attenuator could match the observations under certain circumstances; a choice among them depends, therefore, on the plausibility of the impressed subsidiary conditions. For pressure-induced dipole transitions of CO_2 - N_2 mixtures to explain the observations, a surface pressure in excess of 200 atm is required, according to Barrett and Staelin. This pressure appears incompatible with that derived from infrared and optical data for a convective atmosphere unless the unlikely circumstance prevails that condensation of some atmospheric constituent occurs throughout most of the Cytherean atmosphere (Sagan 1962).

Other inconsistencies arose when water vapor and water clouds jointly provide the millimeter opacity--very low surface pressures and an excessive water vapor mixing ratio are required. However, Barrett and Staelin, following Salomonovich (1964), place the clouds at a higher temperature than would be expected from infrared measurements (e. g., Sinton and Strong 1960). When the cloud thermometric temperatures are brought into agreement with the infrared brightness temperatures, the millimeter spectrum can be reproduced to within observational error without invoking unreasonable water-vapor-mixing ratios or total surface pressures (Sagan and Pollack 1966a; Basharinov and Kutuza 1965).

If the putative Cytherean dust particles are hundreds of microns in diameter--so they Mie scatter as well as absorb microwave radiation--Barrett and Staelin showed that such clouds too can provide a suitable wavelength dependence of brightness temperature. The 100-μ particles must be at the base of the atmosphere, and the particle size must progressively decrease with altitude.

In Paper II, the observed 8-mm phase dependence of brightness temperature was used to discriminate among various potential microwave attenuators. The argument depends on the reality of the 3- and 10-cm phase effects, and on their interpretation in terms of higher surface temperatures for the illuminated hemisphere of Venus. In addition to accounting quantitatively for the phase observations in terms of reasonable surface materials, the theory developed in Paper II also predicts surface temperature variations on Venus which, in turn, imply that the thermal emission at these wavelengths should be between 0. 35 per cent and 2. 0 per cent polarized, depending on the analytic form and magnitude of the latitudinal temperature gradient (Paper I).

Subsequent interferometric observations have yielded at 10.6 cm a polarization of 0.8 ± 0.5 per cent (Clark and Kuz'min 1965), in good agreement with the predictions, and, in turn, tending to confirm the other deductions drawn from the phase observations. When the 8-mm opacity was attributed to CO_2-N_2 mixtures, or to atmospheric water vapor, theory and observation of the phase effect were found to be discordant at 8 mm; but models which invoked clouds of uniform opacity, or atmospheric dust preferentially present in the unilluminated hemisphere, gave results consistent with the observations.

In short, ground-based observations have rendered such atmospheric absorbers as CO_2-N_2 mixtures and H_2O unlikely as sole sources of millimeter opacity on Venus, while models incorporating a cloud layer--particularly a water-cloud layer--or an atmospheric region filled with absorbers or scatterers have survived the preliminary analyses. One objective of the present paper is to further discriminate among alternative millimeter attenuators.

II. THE OBSERVATIONS

In Table 1, we summarize the results of the Mariner 2 observations at 19-mm wavelength. The brightness temperatures T_{Bp} displayed there are the peak temperatures recorded in each scan. The signal-to-noise ratio was observed to decrease sharply away from the center of each scan; we have therefore chosen to consider only the peak temperatures, obtained near the scan centers. The brightness temperatures are corrected for the receiver time constants, and for the fact that the beam is incompletely filled by the planet. (For observations near the limb, the planet did not completely fill the antenna beam.) In addition, these temperatures were derived assuming the surface area instantaneously viewed by the antenna beam was isothermal. In the models we consider below, the brightness temperature T_B will be allowed to vary over the antenna beam. In this case, T_{Bp} and T_B are related by

$$T_{Bp} = \frac{\int_{\varphi} T_B G \, d\Omega}{\int_{\varphi} G \, d\Omega} \quad , \tag{1}$$

where G is the directivity or antenna pattern, and $d\Omega$ is the solid angle at the spacecraft subtended by an element of area on the planetary surface. Since some radiation is, in principle, accepted by the antenna from all directions, the integration should be over all 4π steradians. The tabulated values of T_{Bp} are already corrected for the contribution received from off the planet. The integration is therefore carried out only over the entire planetary disk. The

bulk of the radiation is received by the central lobe of the antenna pattern. From the discussion of Barath et al. (1964), it follows that the directivity can be represented adequately by a gaussian function,

$$G = G_0 \exp \{-(x^2 + y^2)/\sigma^2\} \quad , \tag{2}$$

where x and y are cartesian coordinates perpendicular to the line of sight, and

$$\sigma \cong 2.6 \times 10^{-2} r \quad , \tag{3}$$

where r is the distance from the spacecraft to the surface area viewed. Equation (2) suppresses sidelobes, but radiation entering them makes negligible contribution to the observed brightness temperatures in the present problem. We shall later see that all effects of finite beam width are small; therefore, neglecting sidelobes will introduce errors which are very much of second order.

TABLE 1

PEAK TEMPERATURE OBSERVED BY MARINER 2, 19-mm CHANNEL
(Barath et al. 1964; Jones 1965.)

Scan	Location	Latitude, ξ	Longitude, η	T_{Bp}	sec $\zeta = \mu^{-1}$
1	Dark side	- 6°	137°	490 ± 11° K	1.49
2	Terminator	-18.7°	88°.3	595 ± 12	1.00
3	Bright side	-13.6°	27°	511 ± 14	2.04

The latitudes and longitudes of Table 1 refer to the position of the center of the antenna beam at the moment in each scan of maximum recorded brightness temperature. The zero of latitude is the projection of the orbital plane of Venus on the planetary surface, and is not precisely identical to the equator of the axis of rotation. The zero of longitude is taken to pass through the subsolar point during encounter. These coordinates are used to compute μ^{-1}, the secant of the angle between the line of sight and the local planetary normal at the moment of peak brightness temperature of each scan.

By preflight and in-flight calibration of the microwave radiometer, absolute errors in brightness temperature in the 19-mm channel have been reduced to some 6 per cent, or about 35 K° (Jones 1964, 1965). The errors in brightness temperatures displayed in Table 1 represent the random errors deduced from the scatter of points within a given scan. We will later compare the 19-mm results with those at neighboring frequencies to confirm that the absolute calibration of this Mariner 2 channel is fairly accurate. Because of an inherently lower signal-to-noise ratio, and instrumental difficulties associated with the phase synchrony of chopping (leading to a variable and uncertain baseline), we will not treat the 13.5-mm observations in this discussion. We also note that the reported results (Jones 1964) of the 13.5-mm channel are inconsistent with Earth-based measurements (Gibson and Corbett 1963) at the same frequency, although a secular variability in the brightness temperature at this frequency has been reported (Barrett 1965; Welch and Thornton 1965).

The relative brightness temperatures at the peak of each scan in the 19-mm channel are clearly better known than the absolute peak brightness temperatures. The following discussion is based primarily on these relative values.

As do most radiotelescopes, the Mariner 2 antenna accepted only one component of polarization. If the plane of incidence is defined by the local surface normal (at the point intercepted by the antenna axis), and by the line of sight from spacecraft to surface, the electric vector of the Cytherean emission accepted by the antenna lay perpendicular to the plane of incidence, near the center of each scan. This is a point of some importance; in extreme cases the direction of antenna polarization may make the difference between limb darkening and limb brightening for observations of an identical source.

In the following discussion, we let the symbols $\underline{t}$, $\underline{d}$, and $\underline{b}$ represent, respectively, the terminator, dark-side, and bright-side scans. Any theoretical models of the microwave limb darkening must then reproduce the following data:

$$T_{Bp}(\underline{t}) = 595 \pm 35^\circ K \tag{4}$$

$$\Delta T_{Bp}(\underline{t}, \underline{d}) \equiv T_{Bp}(\underline{t}) - T_{Bp}(\underline{d}) = 105 \pm 25\ K^\circ \tag{5}$$

$$\Delta T_{Bp}(\underline{t}, \underline{b}) \equiv T_{Bp}(\underline{t}) - T_{Bp}(\underline{b}) = 85 \pm 25\ K^\circ \quad . \tag{6}$$

It is significant that the brightness temperatures of both the dark side and the bright side are less than the brightness temperature of the terminator. The observed limb darkening is therefore not simply the result of a higher temperature in the illuminated hemisphere. Since $\Delta T_{Bp}(\underline{t}, \underline{b}) < \Delta T_{Bp}(\underline{t}, \underline{d})$ despite the fact that $\mu^{-1}(\underline{b}) > \mu^{-1}(\underline{d})$, the data immediately suggest that the mean surface temperature on the bright side exceeds that on the dark. We will later extract numerical values for this longitudinal temperature gradient.

III. EQUATIONS OF TRANSFER FOR THE POSTULATED OPACITY SOURCES

a) Overall Strategy

The peak brightness temperature, of, e.g., the terminator scan, is a function of three variables: $T(\lambda; \xi, \eta, z_e)$, the temperature of the effective emitting layer of the Cytherean subsurface at the position and wavelength in question; $\tau(\lambda; \xi, \eta)$, the optical depth of the putative attenuator at the position and wavelength in question; and $e(\lambda; \xi, \eta, \mu)$, the emissivity of the point observed. Here λ represents the wavelength of observation (primarily 19 mm in the ensuing discussion), z_e is the subsurface depth of the layer effectively emitting at wavelength λ, and ξ and η are, respectively, the planetocentric latitude and longitude. The relation among $T_{Bp}(\lambda; \mu; \xi, \eta)$, $T(\lambda; \xi, \eta, z_e)$, and $\tau(\lambda; \xi, \eta)$ is specified by the solution of the equation of radiative transfer for a given opacity source. Once the solution is determined, the measured brightness temperatures will permit us to derive $T(\lambda; \underline{t}, z_e)$ from $\tau(\lambda; \underline{t})$; or, alternatively, $\tau(\lambda; \underline{t})$ from $T(\lambda; \underline{t}, z_e)$ assumed known from previous ground-based observations. We will check our derived value of $\tau(19 \text{ mm}; \underline{t})$ with the value deduced from ground-based observations of the microwave phase effect, and show that the two values are in satisfactory agreement. From $\tau(\lambda; \underline{t})$ and all reasonable values of $T(\lambda; \underline{b}, z_e)$ and $T(\lambda; \underline{d}, z_e)$ we will investigate whether all of the postulated opacity sources are able to reproduce the observed values of $T_{Bp}(\lambda; \mu; \underline{b})$ and $T_{Bp}(\lambda; \mu; \underline{d})$. In the present section we write down the relevant equations of transfer for all postulated opacity sources: CO_2 and N_2 distributed continuously throughout the atmosphere; H_2O, similarly distributed; absorbing dust particles, arbitrarily distributed; an absorbing cloud layer, localized near the top of the atmosphere; and, finally, an array of microwave scatterers distributed in an arbitrary manner throughout the atmosphere.

b) Continuous Distribution of Absorbers

We begin by calculating the brightness temperature of a given locale on Venus when the absorber is distributed continuously and with plane parallel geometry through the atmosphere--as applies to the CO_2-N_2, H_2O, and absorbing dust models. Since the Rayleigh-Jeans approximation to the Planck function is valid at microwave frequencies and Cytherean temperatures, the specific intensity will be proportional to the temperature. The formal solution to the equation of radiative transfer then yields, for this case, the following expression for the brightness temperature detected by an observer at the top of the atmosphere:

$$T_B(\lambda;\mu;\xi,\eta) = e(\mu)\, T(\lambda;\xi,\eta,z_e)\exp[-\tau_s/\mu]$$

$$+ \int_0^{\tau_s} T[\tau(\lambda;\xi,\eta)]\exp[-\tau/\mu]\, d\tau/\mu$$

$$+ [1 - e(\mu)]\exp[-\tau_s/\mu]$$

$$\times \int_0^{\tau_s} T[\tau(\lambda;\xi,\eta)]\exp[-(\tau_s - \tau)/\mu]\, d\tau/\mu \qquad (7)$$

Here $e(\mu)$ is the emissivity for the plane of polarization accepted by the observer, and $\tau_s = \tau_s(\lambda)$ is the total optical depth of the atmosphere in vertical section.

The first term in equation (7) represents the radiation emitted by the subsurface and escaping directly to space through the overlying attenuators. The second term represents the energy radiated directly to space by the attenuator. The third term represents the radiation emitted by the attenuator that is incident on the surface, reflected from it, and transmitted back through the attenuator to space; the factor 1 - e(μ) represents the reflectivity, through Kirchoff's law. We have assumed, in the last term of equation (7), that 19-mm radiation is specularly reflected from the Cytherean surface. Radar observations at 12.5 cm show Venus to be smooth (Carpenter 1964); there is some evidence suggesting that Venus is rough at 3.6 cm (Karp, Morrow, and Smith 1964), but other interpretations of these low signal-to-noise radar observations exist. In any event, the numerical results to be extracted from equation (7) and from analogous subsequent equations are very insensitive to the explicit assumptions regarding surface roughness.

Essential to the solution of equation (7) is knowledge of the dependence of the temperature at each level in the atmosphere on the corresponding optical depth. For each of the three absorbers, the T - τ relation can be written as

$$T = T_s(\tau/\tau_s)^{1/n} \quad , \tag{8}$$

where, for the Cytherean atmosphere, $n \simeq 3.6$ for CO_2-N_2 mixtures, $n \simeq 5.075$ for H_2O vapor with a constant mixing ratio, $n \simeq 3.6$ for dust with a constant mixing ratio, and $n > 3.6$ for dust which tends to settle toward the bottom of the atmosphere (Paper II). The surface temperature is T_s.

The total optical depth at the surface, τ_s, may be expected to vary over the planetary surface if T_s so varies. Since the surface pressure is invariant over the surface (see, e.g., Paper II), the lateral variation of τ_s with T_s may be written

$$\tau_s = \tau_{s0} (T_{s0}/T_s)^{m-n} , \qquad (9)$$

where $m - n = 3.6$ for CO_2-N_2 mixtures, 2.125 for water vapor, and a range of possible values for absorbing dust (Paper II). The quantities τ_{s0} and T_{s0} are the surface optical depth and surface temperature at some reference locale on the planet.

c) Isothermal Clouds

A derivation analogous to that used for equation (7) leads to the following expression for the brightness temperature detected from above when the millimeter opacity is provided by a layer of isothermal clouds:

$$T_B(\lambda;\mu;\xi,\eta) = e(\mu)\, T(\lambda;\xi,\eta,z_e) \exp[-\tau_c/\mu]$$

$$+ T_c\{1 - \exp[-\tau_c/\mu]\}\{1 + [1 - e(\mu)] \exp[-\tau_c/\mu]\} \qquad (10)$$

Here τ_c is the total optical depth of the clouds and the factor $1 - \exp[-\tau_c/\mu]$ represents the cloud emissivity. The cloud temperatures, T_c, is assumed independent, to first order, of position on the disk, in agreement with infrared observations (see, e.g., Sinton and Strong 1960; Murray, Wildey, and Westphal 1963). If the clouds of Venus are water, observations of the infrared limb darkening, of the visible and near infrared reflectivity, and of

the millimeter brightness temperatures can be used to demonstrate that the cloud bottom are only a few tens of degrees warmer than the level observed at 8 to 13 μ (Pollack and Sagan 1965c; Sagan and Pollack, 1966a, 1966b). The 8 to 13 μ brightness temperature of some 234° K (Sinton and Strong 1960) is close to the equilibrium temperature of the planet, deduced from the bolometric albedo. Accordingly, we adopt T_c = 234° K at 19 mm in the following discussion.

d) Pure Isotropic Scattering

We now consider our final opacity source, a plane parallel, but otherwise arbitrary, distribution of purely scattering particles. Since the scatterers contribute no radiation of their own, the observed brightness temperature will depend on the scatterers only through the total optical depth τ_s and will not be a function of the vertical distribution of scatterers. We restrict the present discussion to isotropic scattering; the pronounced anisotropy of the phase function for scattering in the visible and near infrared in the Venus clouds is expected to vanish at longer wavelengths (Pollack and Sagan 1965c; Sagan and Pollack 1966b).

Let $I(\tau_s, \mu', \phi')\, d\Omega'$ be the specific intensity received at the bottom of the atmosphere within a cone of solid angle $d\Omega'$. The quantity ϕ' is the azimuthal angle in a spherical coordinate system with polar axis along the local surface normal; μ' is the arc cosine of the coordinate angle orthogonal to ϕ'. The specific intensity, $I(0, \mu, \phi)$, at the top of the atmosphere in the direction (μ, ϕ) will be related to $I(\tau_s, \mu', \phi')$ by

$$dI(0, \mu, \phi) = I(\tau_s, \mu', \phi') \exp[-\tau_s/\mu'] \, \delta(\mu', \mu) \, \delta(\phi', \phi) \, d\Omega'$$

$$+ (4\pi\mu)^{-1} \mathcal{J}(\mu, \mu') \, I(\tau_s, \mu', \phi') \, d\Omega' \qquad (11)$$

(see Chandrasekhar 1950). Here $\mathcal{T}(\mu, \mu')$ is the transmission matrix for isotropic scattering and $\delta(x, x')$ is the Dirac delta function. Now integrating equation (11) over all solid angles Ω', we obtain the specific intensity at the top of the atmosphere due to radiation incident from all angles at the bottom of the atmosphere, viz.,

$$I(0, \mu, \phi) = I(\tau_s, \mu, \phi) \exp[-\tau_s/\mu]$$

$$+ (4\pi\mu)^{-1} \int\int \mathcal{T}(\mu, \mu') I(\tau_s, \mu', \phi') \, d\mu' \, d\phi'. \qquad (12)$$

Note that in the present case, where thermal radiation is emitted into all angles by the planetary surface, we have generalized from the usual case (Chandrasekhar 1950) of radiation incident on a scattering medium from one direction only. We now proceed to express equation (12) in a form more tractable to numerical studies.

The radiation incident on the scattering layer from below has two components; I_g, the specific intensity of thermal emission directly from the ground, and I_r, the specific intensity of thermal emission from the ground, which has been reflected downward from the scattering layer, and then upward off the surface. After reflection from the scattering layer, the downward-directed specific intensity will be

$$(4\pi\mu')^{-1} \int\int S(\mu', \mu'') [I_g + I_r] \, d\mu'' \, d\phi'' \quad ,$$

where $S(\mu', \mu'')$ is the scattering matrix (Chandrasekhar 1950). By energy conservation, this downward-directed specific intensity must also be $I_r/R(\mu', \phi')$, where $R(\mu', \phi')$ is the reflectivity of the surface. We have again assumed, for analytic convenience, that 19-mm radiation is specularly reflected from the Cytherean surface. Thus we have

$$I_r(\mu', \phi') = (4\pi\mu')^{-1} R(\mu', \phi') \times \iint S(\mu', \mu'') [I_g + I_r] \, d\mu'' \, d\phi'' \quad , \tag{13}$$

an integral equation relating I_r and I_g. The latter depends somewhat on ϕ'', the azimuthal angle for the initially upward-directed radiation, and very little on μ''; I_g is proportional to the product of the emissivity e and the temperature of the effective emitting layer, through the Rayleigh-Jeans law. Since $e_{\parallel}$, the emissivity when the electric vector is parallel to the plane of incidence, differs somewhat from $e_{\perp}$, the emissivity when the electric vector is perpendicular to the plane of incidence, I_g has some dependence on ϕ'. But $e_{\parallel} + e_{\perp}$ is almost independent of μ' from sample numerical calculations using the Fresnel equations; therefore, I_g is similarly independent. Because the surface is hotter than the atmosphere, and because of the low expected surface reflectivities at 19 mm (see Karp, Morrow, and Smith 1964), $\overline{I}_r$, the average value of I_r, is small compared with I_g. Consequently, we may neglect differences among various values of $\overline{I}_r$ obtained when different weighting functions are used in the averaging process. Accordingly, we may rewrite equation (13) as

$$I_r(\mu', \phi') = (1 - e) [\overline{I}_g + \overline{I}_r] \, S(\mu')/\mu' \quad , \tag{14}$$

where the bar denotes a solid angle average, and

$$S(\mu')/\mu' \equiv \frac{1}{2} \int_0^1 S(\mu', \mu'')\, d\mu'' \quad . \tag{15}$$

If, further, we multiply equation (14) by $\mu' d\mu' d\phi'$ and carry out the double integration, we find

$$\overline{I}_r = [\Xi - 1]\, \overline{I}_g \quad , \tag{16}$$

where

$$\Xi \equiv [1 - \overline{R}\,\overline{S}]^{-1} \tag{17}$$

and

$$\overline{S} = 2 \int_0^1 S(\mu')\, d\mu' = \int_0^1 \int_0^1 \mu' S(\mu', \mu'')\, d\mu'\, d\mu'' \tag{18}$$

Values of $\overline{S}$ as a function of the extinction optical depth of the scattering layer have been tabulated by Chandrasekhar and Elbert (1952).

Returning now to equation (12), and replacing $I(\tau_s, \mu', \phi')$ by $I_g + I_r$, we find, analogously,

$$I(0, \mu, \phi) = [I_g + I_r] \exp[-\tau_s/\mu] + [\overline{I}_g + \overline{I}_r]\, \mathcal{T}(\mu)/\mu \quad , \tag{19}$$

where

$$\mathcal{J}(\mu)/\mu \equiv \frac{1}{2} \int_0^1 \mathcal{J}(\mu, \mu')\, d\mu' \quad . \tag{20}$$

Substituting for I_r and $\bar{I}_r$ from equations (14) and (16), we write equation (19) as

$$I(0, \mu, \phi) = [I_g + (1 - e)\, \Xi\, \bar{I}_g\, S(\mu)/\mu]\ \exp[-\tau_s/\mu] + \Xi\, \bar{I}_g\, \mathcal{J}(\mu)/\mu \quad . \tag{21}$$

Finally, equation (21) can be converted from an expression in specific intensity to one in brightness temperature:

$$T_B(\lambda; \mu, \phi; \xi, \eta) = T(\lambda; \xi, \eta; z_e) \times \{[e + (1 - e)\, \bar{e}\ \Xi\, S(\mu)/\mu] \exp[-\tau_s/\mu]$$

$$+ \Xi\, \bar{e}\, \mathcal{J}(\mu)/\mu\} \quad . \tag{22}$$

IV. APPROXIMATIONS AND SPECIFICATION OF PARAMETERS

a) Approximations for the Brightness Temperature

Equations (7), (10), and (22) give the functional form of the brightness temperature for each assumed opacity source. There are five reasons that T_B will vary from one scan to the next:

1) The emissivity will vary from scan to scan because $e = e(\mu)$.

2) There may be a real variation of dielectric constant with position on the surface. We will assume, however, that the dielectric constant does not vary over the disk.

3) The equivalent atmospheric optical depth viewed by the spacecraft is proportional to μ^{-1}. Both factors 1) and 3) produce a decrease of T_B with increasing μ^{-1}.

4) The atmospheric optical depth may vary with position on the disk, for example because the opacity may be temperature-dependent. Equation (9) gives the explicit dependence of τ_s on T_s for CO_2-N_2 mixtures and for water vapor. For these models, τ_s will be largest on the dark side and smallest on the bright side. Thus, through the temperature dependence of opacity, a latitudinal surface-temperature gradient, with cooling toward the poles, will help to lower T_B in both hemispheres; but, for a fixed terminator temperature, a longitudinal gradient of surface temperature will help to lower T_B on the dark side and raise it on the bright side. For the remaining models (absorbing dust, a cloud layer, and a scattering aerosol) there is no a priori constraint on the dependence of optical depth on surface locale. If there were no other relevant observational data, it would be a trivial problem to explain the Mariner 2 observations by judiciously choosing $\tau_s(\xi, \eta)$ for these three models, a point we discuss in more detail later.

5) A final factor influencing the variation of T_B from scan to scan is the longitudinal gradient of surface temperature directly; since T_s is expected to be greater on the bright side, this will tend directly to increase T_B in the illuminated hemisphere.

We now consider the use of equation (1) to relate the theoretical brightness temperatures T_B to the observed peak values T_{Bp}. As given by equations (7), (10), and (22), the brightness temperature may be represented as

$$T_B = v(\mu, \tau_s) + w(\mu, \tau_s)\, T(\lambda; \xi, \eta, z_e) \quad . \tag{23}$$

For equations (7) and (22), $v(\mu, \tau_s) = 0$. We now explicitly ignore in equation (23) the variation of τ_s, the optical depth, and of $T(\lambda; \xi, \eta; z_e) \equiv T_g$, the temperature of the effective subsurface emitting layer over the beam width of the antenna. A convenient analytic representation of the limb darkening over the beam width because of the dependence on μ is then

$$T_B = T_B(\mu = \mu_0)\, (\mu/\mu_0)^{a} \quad , \tag{24}$$

where μ_0 is the value of μ at the center of the beam. Application of this representation to the various opacity models shows that a is very close to a constant over a wide range in μ. If, then, we substitute equations (23) and (24) into equation (1), and make use of equations (2) and (3), we formally obtain

$$T_{Bp} = T_B(\mu = \mu_0)\, Q(a) \quad , \tag{25}$$

where $Q(a)$ is always slightly less than unity. In Table 2 are shown the computed values of $Q(a)$ for two representative values of a, and for each of the three scans. Thus T_{Bp} differs from $T_B(\mu = \mu_0)$ by at most 25 K°, an amount comparable to the probable errors of measurement [cf. equations (4)-(6)], and for the accuracy of the present problem, equation (25) should be adequate.

TABLE 2

REPRESENTATIVE VALUES OF $Q(a)$

Scan	t	d	b
a/μ_0	1.00	1.49	2.04
0.25	0.997	0.979	0.975
0.50	0.995	0.965	0.962

We now consider what value should be assigned $\langle T_g \rangle$ the average ground temperature over the beam. It is clear that $\langle T_g \rangle \simeq T_g(\mu = \mu_0)$. The ground temperature decreases poleward and increases toward the equator; the latitudinal average will be close to the value at beam center. A similar statement holds for the longitudinal temperature variation. To obtain a quantitative estimate of $\langle T_g \rangle$, we have calculated the differences in temperature between a point at the center of the beam, and at four points, north, south, east, and west of beam center, at which the directivity G had fallen to 1/e its maximum value. To maximize the deviation of $\langle T_g \rangle$ from $T_g(\mu = \mu_0)$, we have used an extreme form for the variation of temperature with latitude, viz., $(1 - a|\sin \xi|)$, where a is a measure of the latitudinal gradient. In particular, we choose the following analytic form for the dependence of $T(\lambda; \xi, \eta; z_e) \equiv T_g$ on the latitude ξ and the longitude η:

$$T(\lambda; \xi, \eta, z_e) = (1 - a|\sin \xi|)\, T_0(z_e, 0)$$

$$+ (1 - |\sin \xi|) \cos \eta \; T_1(z_e, 0) \qquad (26)$$

Note that $\eta = 0^{\circ}$ occurs at the subsolar point. To sufficient accuracy for the present problem,

$$T_0(z_e, 0) \simeq T_0(0, 0) \text{ and } T_1(z_e, 0) \simeq T_1(0, 0) \quad .$$

From interferometric studies (Paper I; Clark and Kuz'min 1965) it follows that $a \simeq 0.30$. A discussion of surface temperature variations similar to equation (26), and specific numerical values of $T_0(0, 0)$ and $T_1(0, 0)$ for $a \simeq 0.30$ may be found in Paper I. After computing T_g for the five representative points near the peak of each scan, we have calculated the beam average of T_g. We find that, to within 10 K°, $\langle T_g \rangle = T_g(\mu = \mu_0)$. Considering the extreme analytic form adopted for the temperature variation, we will henceforth neglect the difference between $\langle T_g \rangle$ and $T_g(\mu = \mu_0)$.

Thus, it is possible to reduce considerably the labor of computing T_{Bp} without appreciable loss of accuracy. We calculate $T_B(\mu = \mu_0)$, from equation (23), determine α for $\mu = \mu_0$, and then use Table 2 to find $Q(\alpha)$ and T_{Bp}.

b) Specification of Emissivities and Dielectric Constants

For a point near the center of the beam, we must use $e_\perp$ the value of the emissivity with the E vector normal to the incident plane. For other positions in the beam, e will be a hybrid of $e_{\parallel}$ and $e_\perp$, with $e_\perp$ dominating. In equation (22), $\bar{e}$ implies an average over both $e_\perp$ and $e_{\parallel}$. We must, therefore, specify the auxiliary functions e and $\bar{e}$.

Under the usual assumptions of plane parallel geometry and equality of the magnetic permeabilities of the vacuum and of the surface, a combined Kirchhoff-Fresnel equation can be written:

$$e_{\perp} = 1 - R_{\perp} = 1 - \left[\frac{\mu - (\epsilon - 1 + \mu^2)^{1/2}}{\mu + (\epsilon - 1 + \mu^2)^{1/2}}\right]^2 , \qquad (27)$$

where ϵ is the real part of the surface dielectric constant. Here arc cos μ is again the angle between the line of sight and the local normal.

Even when the finite beam width is taken into account, it is still appropriate to use only $e_{\perp}$ to calculate T_{Bp}, as we now undertake to demonstrate. The $\underline{E}$ vector accepted by the Mariner 2 antenna lay perpendicular to the orbital plane of Venus and, of course, perpendicular to the line of sight of the spacecraft. Consider a cartesian coordinate system (x, y, z) with origin at the center of the planet. The antenna accepts an electric vector of an incoming wave train polarized in the y direction. The direction to the spacecraft is along the z axis. If $|\underline{n}|$ is the unit vector normal to the plane of incidence, and cos $\chi \equiv |\underline{y}| \cdot |\underline{n}|$, then it is easy to show (cf. Paper I) that

$$E_y^2 \propto [e_{\parallel} \sin^2 \chi + e_{\perp} \cos^2 \chi] \qquad (28)$$

so that the power emissivity of the component of E accepted by the antenna is

$$e = e_{\parallel}\left(\frac{y^2}{x^2 + y^2}\right) + e_{\perp}\left(\frac{x^2}{x^2 + y^2}\right) \qquad (29)$$

For the center of the terminator scan, $\mu = 1$ and $e_{\parallel} = e_{\perp}$. Calculations using equations (2) and (3) show that for other positions on the disk contributing significantly to the received signal on this scan, $e_{\parallel}$ and $e_{\perp}$ do not differ appreciably; in this sense, we may set $e = e_{\perp}$. For the other two scans $e_{\parallel}$ and $e_{\perp}$ differ significantly. At the center of these scans, $y = 0$, and $e = e_{\perp}$. Sample calculations show that, to an accuracy of one per cent, $e = e_{\perp}$ for the entire antenna pattern in these scans as well. This can be seen in a simple way by noting that $x = 0.67 > R_{\varphi}$ for scan d and $0.80\ R_{\varphi}$ for scan b; in both cases, $\sigma \simeq 0.17 R_{\varphi}$ where R_{φ} is the radius of Venus. Thus, $x^2(x^2 + y^2)^{-1} \simeq 1$ always and $y^2(x^2 + y^2)^{-1} \simeq 0$ always over those regions contributing significantly to the received signal.

To evaluate equation (27), we must specify a value or range of values for the dielectric constant. Radar observations at 12.5 cm yield a value of $\epsilon \simeq 3.6$ (Carpenter 1964, 1966), and similar, but somewhat larger values are deduced from the reflectivities at longer wavelengths. However, the reported reflectivity at 3.6 cm is 0.009 ± 0.003 (Karp et al. 1964). One interpretation (Paper II) of the decline in radar reflectivity toward shorter wavelengths is a corresponding decline in the dielectric constant. In this case $\epsilon(3.6\ \text{cm}) \simeq 1.45$. Other interpretations of the low reflectivity have been proposed, however (Paper II). In our calculations we will employ both values: $\epsilon(19\ \text{mm}) = 3.6$, and $\epsilon(19\ \text{mm}) = 1.45$. Note that the 3.6-cm radar results refer to a depth about equal to $z_e(19\ \text{mm})$.

To this point in the discussion, we have assumed Venus to be smooth at 19 mm, and so have neglected depolarization effects due to surface roughness. The rougher the surface, the closer are $e_{\perp}$ and $e_{\parallel}$. Carpenter (1966) has discussed the polarization of initially polarized 12.5 cm CW radar after reflection from Venus. He assumes that the reflected polarized power consists of two components, that returned with no depolarization by quasi-smooth areas of the disk, and that returned with about 50 per cent depolarization from areas which are rough at this radar frequency. Carpenter

concludes that about 7.5 per cent of the Cytherean surface is rough in this sense, but this conclusion depends on his implicit assumption that the reflectivity R_r of the rough fraction of the disk equals $R_s(\theta = 0°)$, the normal incidence reflectivity of the smooth fraction of the disk. Actually, since the effects of surface roughness generally involve both multiple scattering and multipole reradiation of the incident power, we expect $R_r > R_s(\theta = 0°)$. In the limiting case $R_r = 1$, a recalculation of Carpenter's results shows only about 1 per cent of the surface to be rough. There are other uncertainties in these calculations, including the assumed depolarization of rough areas, and the assumed scattering phase functions of rough and smooth terrains. With these uncertainties, the fraction of the surface which is rough at 12.5 cm lies between 1 and 7.5 per cent, and has little influence on the deduced surface dielectric constant.

Interferometric studies of the polarization of Cytherean thermal emission, performed by Clark and Kuz'min (1965) indicate a significantly lower dielectric constant (about 2.5) at 10.6 cm than the radar observations at 12.5 cm indicate. If the difference in results is attributed to depolarization by surface roughness, we calculate that a depolarization of about 40 per cent is required. On the other hand, these interferometric observations admit other possible interpretations, in terms, e.g., of atmospheric or cloud opacity, or surface inclination near the limbs to which the polarization is particularly sensitive. Forty per cent depolarization appears to be an upper limit to the depolarization allowed by the radar and interferometric observations.

V. OPACITIES AND TEMPERATURES FROM GROUND-BASED OBSERVATIONS

a) Constraints on the 19-mm Opacity from the 8-mm Phase Effect

Observations of the variation of brightness temperature with phase angle at 8-mm wavelength place constraints on the 19-mm variation of opacity over the disk in the cloud, distributed scatterer, and distributed absorber models. Without such constraints, these models could be made to match the Mariner 2 observations trivially, simply by selecting an appropriate opacity for each scan. If the surface were isothermal, we could expect the opacities to be independent of position on the disk. The case of interest, however, concerns large temperature gradients, as probably exist (Papers I and II). If we average equations (7), (10), and (22) over solid angles, we obtain disk-integrated brightness temperatures $\overline{T}_B$ to compare with the phase-effect observations. For the cloud and distributed scatterer models, we find

$$\overline{T}_B(\text{clouds}) = 2\,\overline{e}\,T_g\,E_3(\tau_c) + T_c\left[1 - 2\,(1+\overline{e})\,E_3(\tau_c)\right]$$

$$- 2\,T_c\,(1-\overline{e})\,E_3(2\tau_c) \qquad (30)$$

where

$$E_3(\tau) \equiv \int_0^1 \mu\, e^{-\tau/\mu}\, d\mu \ , \qquad (31)$$

and

$$\overline{T}_B(\text{scatterers}) = \overline{e}(1 - \overline{S})\, T_g \left[1 + \frac{\overline{R}\,\overline{S}}{1 - \overline{R}\,\overline{S}}\right] . \qquad (32)$$

Since $\overline{R}$ is about 0.1, from the radar observations, and $\overline{S} \sim 0.1$ for the range of optical depths appropriate to Venus and 19 mm (see Chandrasekhar and Elbert 1952) we see that the factor enclosed in square brackets in equation (32) is close to unity. Thus, whether the surface is smooth or rough has little effect on numerical results derived from equation (32). The form of the equation shows that, when $\overline{R}\,\overline{S} \ll 1$, the Russell-Bond albedo for this problem is simply $\overline{S}$.

In the distributed absorber models it follows from equation (7) that $\tau_s \gg 1$ at 8 mm. This can be seen readily from a simplified form of equation (7),

$$T_B \simeq T_g \exp[-\tau_s/\mu] + \{1 - \exp[-\tau_s/\mu]\}\, T_a , \qquad (33)$$

where T_a is some effective atmospheric radiating level at 8 mm. We have already seen [equation (8)] that $\tau \propto T^n$ in this model, where $n \geq 3.6$. Thus, if τ_s were small, T_a and T_g would differ negligibly--even including effects of temperature discontinuities at the planetary surface--and it would be impossible to reduce T_B from the expected value of $T_g \sim 700°$ K to the observed value $\sim 400°$ K. But if τ_s were large, T_g and T_a could differ substantially and $T_B \ll T_g$ could, in this model, be understood. Since $\tau_s \gg 1$, T_B (8 mm) must correspond approximately to the temperature at the $\tau = 2/3$ level of the atmosphere for this frequency. It then follows from equation (8) that the ratio, $\overline{\tau}_{s1}/\overline{\tau}_{s2}$, of the disk-averaged optical depths at

two phase angles are related to the average surface temperatures $\overline{T}_s$ and 8-mm brightness temperatures $\overline{T}_B$ by

$$\overline{\tau}_{s1}/\overline{\tau}_{s2} = (\overline{T}_{s1}\,\overline{T}_{B2}/\overline{T}_{B1}\,\overline{T}_{s2})^n \quad , \tag{34}$$

where $n = 3.6$ for a constant vertical mixing ratio of absorbing dust, and $n > 3.6$ if the dust tends to settle toward the bottom of the atmosphere.

Recent measurements of the 8-mm phase effect have been made by Basharinov, Vetukhnovskaya, Kuz'min, Kutuza, and Salomonovich (1964) and by Copeland and Tyler (1964); these observations agree with each other within the probable errors of measurement. A very conservative summary of these observations is that $\overline{T}_B$ (8 mm) for the illuminated hemisphere of Venus is between 0 and 120 K° higher than $\overline{T}_B$ (8 mm) for the dark side. At 90° phase angle, $\overline{T}_B$ (8 mm) is about 425° K. Thus, even with crude information on surface temperatures, equations (30), (32), and (34) permit some limits to be set on $\tau(\underline{b})/\tau(\underline{d})$ for the isothermal cloud, distributed scatterer, and distributed absorber models. For example, if we choose, from observations at longer wavelengths, $\overline{T}_g(\underline{b}) \simeq 800°$ K and $\overline{T}_g(\underline{d}) \simeq 650°$ K (cf. Papers I and II) we find

$$\text{clouds:} \qquad 0.7 \leq \tau(\underline{b})/\tau(\underline{d}) \leq 1.7 \tag{35}$$

and

$$\text{scatterers:} \quad 0.9 \leq \tau(\underline{b})/\tau(\underline{d}) \leq 1.7 \quad . \tag{36}$$

Thus, in these models, the maximum variation of attenuator opacity from bright to dark sides is small. Because of the large value of n, equation (34) permits larger variations in $\tau(\underline{b})/\tau(\underline{d})$ in the distributed absorber models.

In practice, we will derive for each model the optical depth at 19 mm--a parameter relevant to the Mariner 2 observations--by reproducing the observed brightness temperature of the terminator scan. Nevertheless, it will be useful to obtain an independent estimate of τ (19 mm), both to check the asserted accuracy of the Mariner 2 calibration, and to establish how well these 19-mm observations, corrected for phase and for disk-integration, fit the Venus microwave spectrum as determined on Earth at other wavelengths. Using equations (30), (32), and

$$\overline{\tau}_s \simeq \frac{2}{3}\left(\overline{T}_s/\overline{T}_B\right)^n \tag{37}$$

for the continuously distributed absorber models, and quadrature values of $\overline{T}_B \simeq 425°K$ and $\overline{T}_s \simeq 700°K$ (Papers I and II), we derive $\overline{\tau}$(8 mm) for each model. For the CO_2-N_2 and H_2O absorbers, $\tau \propto \lambda^{-2}$; thus, once $\overline{\tau}_s$ (8 mm) is found from equation (37), $\overline{\tau}_s$ (19 mm) is readily derived. The observed spectral distribution of $\overline{T}_B$ for $\lambda < 3$ cm implies $\tau \propto \lambda^{-2}$ approximately, provided ϵ is frequency-independent. However, the dielectric constant at 3 cm may lie between 1.45 and 3.6, its value at longer wavelengths, as we have already discussed. In the cloud and distributed scatterer models, this possible variation of ϵ with λ allows $\tau(\lambda)$ dependences varying from λ^{-1} to λ^{-2}, while still reproducing the observed $T_B(\lambda)$.

In Table 3 are displayed our estimates for τ(19 mm) derived from τ(8 mm) for each model. In the distributed absorber model it is easy to show that, if the mixing ratio of absorbing dust to gas goes as the s^{th} power of the pressure, then $n = 3.6\,(1+s)$ (cf. Pollack and Sagan 1965c).

TABLE 3

ESTIMATES OF $\bar{\tau}$(19 mm) AT QUADRATURE FROM EARTH-BASED MEASUREMENTS OF $\bar{\tau}$ (8 mm)

		MODEL			
Surface dielectric constant (8-19 mm emitting levels)	λ-dependence of τ	Absorbing dust (s=0) or uniformly mixed CO_2-N_2	Absorbing dust (s=0.4) or uniformly mixed H_2O	Isothermal clouds T_c=234° K	Arbitrarily distributed scatterers
3.6	λ^{-2}	0.9	1.6	0.07	0.12
1.45	λ^{-2}	0.9	1.6	0.09	0.15
1.45	λ^{-1}	--	--	0.20	0.35

b) Estimates of Surface Temperatures Appropriate for the Mariner 2 Scans

We now obtain estimates of surface and subsurface temperatures appropriate for each scan using ground-based observations at longer wavelengths alone. As with the opacities, a comparison of Mariner 2 with ground-based observations of temperature will prove useful. We have already mentioned the inferences drawn from phase-effect observations about large longitudinal surface temperature gradients on Venus, and, from interferometric observations, of large latitudinal gradients. In Papers I and II, we

have given four possible analytic forms for the surface temperature distribution. Each form satisfies the formal solution of the heat conduction equations for rotational phase symmetry (Paper I), viz.,

$$T(0, \xi, \eta, t) = T_0(0, \xi) + T_1(0, \xi) \cos (a + \eta) \quad . \tag{38}$$

Here $T(0, \xi, \eta, t)$ is the surface thermometric temperature (depth zero) at the specified latitude, longitude, and time; $T_m(0, \xi)$ is the m^{th} Fourier coefficient of the diurnal variation of surface temperature, and a is the surface phase lag, and is to be distinguished from the exponent of the limb-darkening law (24). Note that the only longitudinal dependence is as a term in the argument of the cosine in equation (38), and that the equation is defined for the longitude convention that $\eta = 0°$ corresponds to the subsolar point. The four specified analytic forms for $T_m(0, \xi)$ are

$$T_0^{(i)}(0, \xi) = [1 - a^{(i)} + a^{(i)} \cos \xi] \; T_0(0, 0) \tag{39}$$

$$T_0^{(ii)}(0, \xi) = [1 - a^{(ii)} \; |\sin \xi|] \; T_0(0, 0) \tag{40}$$

$$T_1^{(i)}(0, \xi) = [\cos \xi] \; T_1(0, 0) \quad . \tag{41}$$

$$T_1^{(ii)}(0, \xi) = [1 - |\sin \xi|] \; T_1(0, 0) \quad . \tag{42}$$

Here $a^{(i)}$ and $a^{(ii)}$ are indices of the latitudinal temperature gradient, and have values $a^{(i)} \simeq a^{(ii)} \simeq 0.30$ implied by microwave interferometry of Venus (Clark and Kuz'min 1965, and Paper I). Values of the Fourier coefficients $T_0(0, 0)$ and $T_1(0, 0)$ can be obtained from equations (101) and (102), and Table 7 of Paper II. Using these results we have computed, in Table 4 of the present paper, the predicted peak surface temperatures for each of the three Mariner 2 scans. The values displayed are means over the four analytic forms, equations (39) through (42), and the errors shown indicate the extent to which the various forms agree.

To connect brightness temperatures at different frequencies (referring, therefore, to different effective emitting levels), or brightness temperatures with surface temperatures, a simultaneous solution of the equations of heat conduction and radiative transfer is required For the case of rotational phase symmetry applicable to Venus, this solution can be written for the thermometric temperature of the subsurface layer effectively emitting 19-mm radiation as (cf. Paper II)

$$T_g(19\text{ mm}) = T_0(0, \xi) + [1 + 1.9\gamma + 1.8\gamma^2]^{-1/2}$$

$$\times T_1(0, \xi) \cos [-\psi + \eta + \alpha] \quad , \qquad (43)$$

where γ is the ratio of electromagnetic to thermal skin depths and $\psi = \psi(\gamma)$ is the progressive phase retardation of the propagating thermal wave. From values of γ at 3 cm, and estimates of its wavelength dependence, we find $\gamma(19\text{ mm}) = 0.2 \pm 0.1$ and $\psi(\gamma) = 8^\circ.5 \pm 3^\circ.5$; the value of α is expected to be negligibly small (Paper II). From equation (43) and the range of adopted analytic forms of the surface temperature distribution, we can now compute mean values of $T_g(19\text{ mm})$ also shown in Table 4. The values of

T_s and T_g(19 mm) do not greatly differ; 19-mm radiation is emitted from a level quite close to the Cytherean surface. Note that errors due to the assumed temperature distribution are least for the terminator scan. We will, therefore, begin our comparison of these predicted and the Mariner 2-observed brightness temperature for that scan.

TABLE 4

ESTIMATES OF T_s AND T_g(19 mm) APPROPRIATE FOR THE MARINER 2 SCANS, CALCULATED FROM GROUND-BASED OBSERVATIONS

Scan	T_s	T_g(19 mm)
d	620 ± 45° K	630 ± 60° K
t	730 ± 5	700 ± 15
b	885 ± 25	845 ± 40

VI. COMPARISON OF THE MODELS AND THE OBSERVATIONS

Using equation (25) and Table 2, we can calculate the brightness temperature at the center of each Mariner 2 scan. For each model, we force the attenuator to account for the difference between the observed peak brightness temperature of the terminator scan and the predicted subsurface emission temperature of the same scan [T_g(19 mm) $\simeq$ 700° K of Table 4]. This procedure specifies the optical depth for the model in question. With this value of τ we ask whether the observed brightness temperature of the other two scans can be reproduced; i.e., we seek values of $T_g(\underline{b})$ and $T_g(\underline{d})$ such that the observed values of $T_B(\underline{b})$ and $T_B(\underline{d})$ are accounted for. In order for a model to prove unsuccessful, we require it to fail to reproduce the observations for all reasonable surface temperature distributions--including the unlikely case of an isothermal surface. In this manner, the rejection of a model will not depend on the validity of other analyses, such as the predicted variation of T_s and T_g with position as given in Table 4. In accord with the discussion of equations (35) and (36) above, we initially neglect possible systematic variation of the quantity of attenuators between the bright and dark sides of Venus. We will later consider the effects of varying the abundance of attenuators with position, for the distributed absorber and distributed scatterer models, within the constraints established by the phase effect.

Our comparison of results is summarized in Table 5. The symbols $\Delta T_B(\underline{t}, \underline{d})$ and $\Delta T_B(\underline{t}, \underline{b})$ are defined by equations (5) and (6). For a range of possible values of the analogous parameters $\Delta T_g(\underline{t}, \underline{d})$ and $\Delta T_g(\underline{t}, \underline{b})$, we see that the CO_2-N_2, water vapor, and distributed absorbing dust models are unable to reproduce the observations; the 234° K cloud and distributed scatterer models have no such attendant difficulties.

TABLE 5

PREDICTED AND OBSERVED VALUES OF T_B (19 mm)

	ϵ	τ	$T_g(t)$ (° K)	$T_g(d)$ (° K)	$T_g(b)$ (° K)	$T_B(t)$ (° K)	$\Delta T_B(t, d)$ (K°)	$\Delta T_B(t, b)$ (K°)
Observed by Mariner 2	--	--	--	--	--	595 ± 35	105 ± 25	85 ± 25
Predictions of models:								
Absorbing dust with s = 0	1.45	0.9	700	700	700	590	45	80
or CO_2-N_2 mixture	3.6	0.9	700	700	700	580	45	80
Absorbing dust with s = 0.4	1.45	1.6	700	700	700	575	45	80
or water vapor	3.6	1.6	700	700	700	575	45	80
Absorbing dust with s = 0	3.6	0.9	700	600	800	580	120	10
Absorbing cloud T_c = 234° K	3.6	0.10	700	675	835	595	105	85
	3.6*	0.10	700	635	740	595	105	85
	1.45	0.25	700	635	760	590	105	85
Distributed scatterers	3.6	0.15	700	670	795	590	105	85
	3.6*	0.15	700	640	730	590	105	85
	1.45	0.33	700	635	725	595	105	85

*With 40 per cent depolarization.

In the remainder of this section we consider the unsuccessful CO_2-N_2, water vapor, and distributed absorbing dust models. These models clearly fail for an isothermal planet. If we allow for a more plausible temperature distribution, we find that $T_B(\underline{b})$ increases and $T_B(\underline{d})$ decreases. This comes about in two ways, because of the variation in surface temperature directly, and because of the dependence of opacity on surface temperature [cf. equation (9)]. Our estimate of the surface temperature variation--given, e.g., in Table 4--shows that the temperature differences between bright side and terminator exceeds that between dark side and terminator. Thus, as we allow for a nonisothermal surface, $\Delta T_B(\underline{t}, \underline{b})$ will be decreased more than $\Delta T_B(\underline{t}, \underline{d})$ will be increased, and agreement with the Mariner 2 observations cannot be secured. The optical depths derived in these calculations are in excellent agreement with those previously estimated from ground-based observations [cf. Table 3]; we are therefore unlikely to have made a serious error in extracting the value of τ from the Mariner 2 observations. We therefore conclude that CO_2-N_2 and water vapor are not the primary sources of millimeter opacity, a conclusion already reached from an examination of the 8-mm phase effect (Paper II).

Consider now the model in which absorbing dust is distributed continuously through the Cytherean atmosphere. It is clear that, regardless of our choice of the pressure-dependent parameter, s, we again encounter the same difficulties intrinsic to the unsuccessful CO_2-N_2 and water vapor models. However, we here have more freedom to vary the opacity with position over the planet. Might there be some felicitous distribution of dust which secures agreement with the Mariner 2 data? For the opacity to vary significantly, there must be substantial temperature gradients across the planet. Equation (34) relates the optical depths at two locales on Venus to the corresponding

surface temperatures and brightness temperatures. The fifth model entry in Table 5 shows the predicted values of $\Delta T_B(\underline{t}, \underline{d})$ and $\Delta T_B(\underline{t}, \underline{b})$ for a substantial lateral temperature gradient, but for uniform opacity. As we allow for such gradients, we find that, e. g., $T_s(\underline{b})/T_s(\underline{t}) > T_B(\underline{b})/T_B(\underline{t})$, and so, from equation (34), $\tau(\underline{b}) > \tau(\underline{t})$. It is thus possible to bring $\Delta T_B(\underline{t}, \underline{b})$ into agreement with observation. However, at the same time, $\tau(\underline{d})$ will be significantly decreased, and the value of $\Delta T_B(\underline{t}, \underline{d})$ predicted by the model will be much smaller than observed. Even with the many degrees of freedom which the distributed absorbing dust model possesses, extreme difficulties are encountered in attempting to force a fit with observation. Accordingly, we reject this model as unsatisfactory.

We have shown that the terminator scan sees essentially $\epsilon_{\parallel}$. Thus, as we scan from the center of the disk, e will increase until it reaches unity at the Brewster angle, arctan $\epsilon^{1/2}$. However, the 19-mm observations show no increase in T_B toward the Brewster angle, and $T_B(\text{Brewster}) \leq 615^\circ$ K. To test the compatibility of our two successful models, we have computed $T_B(\text{Brewster})$ for them, letting $T_s(\text{Brewster}) = 700^\circ$ K. Because of the slant paths involved, the results were in all cases in accord with the observational upper limit of 615° K. In actuality, $T_s(\text{Brewster})$ must be less than 700° K because of the poleward decrease of surface temperature--a circumstance that further lowers $T_B(\text{Brewster})$ and strengthens our conclusions. Thus the successful models are compatible with the absence of Brewster highlights.

VII. UPPER LIMITS TO THE SURFACE PRESSURE AND WATER-VAPOR ABUNDANCE ON VENUS

We have found that neither water vapor nor carbon dioxide-nitrogen mixtures are the major sources of opacity at 19 mm. This result allows us to set upper limits on P_s, the total surface pressure, and on w_{H_2O}, the total water-vapor abundance on Venus. For CO_2-N_2 or H_2O vapor to be the sole sources of opacity, τ_s (19 mm) was found to be 0.9 and 1.6, respectively. We can consider that the actual optical depth for these opacity sources is less than one-third of these values, viz.,

$$\tau_s(19 \text{ mm}, H_2O) \leq 0.5$$

$$\tau_s(19 \text{ mm}, CO_2\text{-}N_2) \leq 0.3 \quad .$$

For those successful models with $\epsilon = 3.6$, we found that the surface depolarization inferred from ground-based observations would not be as great as 40 per cent. If we attribute all the depolarization to gaseous atmospheric absorbers, we have

$$\exp[-\tau_s/\mu] \simeq \exp[-2\tau_s] < 0.40 \quad ,$$

or

$$\tau_s(19 \text{ mm}, H_2O \text{ or } CO_2\text{-}N_2) < 0.25 \quad .$$

We now relate τ_s(19 mm, CO_2-N_2) to surface pressure and thereby obtain an upper bound on P_s. Both CO_2 and N_2 undergo pressure-induced dipole transitions at sufficiently elevated pressures. At a given pressure, CO_2 is a more efficient pressure-induced absorber than N_2. From measurements of mixtures of CO_2 and N_2 by Ho, Osborn, and Thaddeus (1963; see also, Barrett and Staelin 1964) over a range of pressures up to 60 atm, and a range of temperatures up to 400°K, the absorption cross section of the mixture, per unit volume, may be written as

$$\kappa\,(CO_2, N_2) = 1.5 \times 10^{-8}\, \nu_G^{\,2}\, P^2\, T_{100}^{\,-4.6}\, H\left(q_{CO_2}\right) \quad \text{cm}^{-1} \tag{44}$$

where

$$H(q) = q_{CO_2}^{\,2} \left[1 + 0.07\left(\frac{1 - q_{CO_2}}{q_{CO_2}}\right) + 0.012\left(\frac{1 - q_{CO_2}}{q_{CO_2}}\right)^2\right] \tag{45}$$

and ν_G is the microwave frequency in gigacycles, P is the pressure in units of atmospheres, T_{100} is the temperature in units of 100°K, and q_{CO_2} is the ratio of the CO_2 partial pressure to the total pressure of the CO_2 - N_2 mixture. More recent work has extended the applicability of equations (44) and (45) over a larger temperature and pressure range (Thaddeus, 1965). Note that even for the case of $q_{CO_2} = 0$ (no carbon dioxide), $H\left(q_{CO_2}\right) > 0$ because of N_2 pressure-induced transitions.

The absorption coefficient κ is related to τ_s by $\tau_s = \int \kappa \, dz$, where dz is a differential element of vertical distance. A τ - P relation can be derived by integrating this equation. We convert from a z-integration to a T-integration by noting that the lapse rate will be adiabatic and approximately constant with altitude (cf. Sagan 1962); and use Poisson's law to relate P and T. Setting the surface temperature equal to 700° K, the lapse rate equal to 8.4 K°/km, and the ratio of specific heats equal to 1.38, we find

$$P_s \simeq 30 \left[\tau_s (19 \text{ mm})/H(q_{CO_2})\right]^{1/2} \text{ atm} \qquad (46)$$

The coefficient of equation (46) depends on the assumption $T_s = 700°$ K; but since $P_s \propto T_s^{1.8}$ in this derivation, variations of T_s by some tens of degrees will have little influence. Estimates of q_{CO_2} range from 0.05 (Spinrad 1962a) to perhaps one-tenth this value (Chamberlain 1965). For $q_{CO_2} = 0$ and $\tau_s (19 \text{ mm}) < 0.3$, we find

$$P_s < 150 \text{ atm} \qquad (47)$$

Using $q_{CO_2} = 0.05$ and $\tau_s (19 \text{ mm}) < 0.25$, we could set a slightly lower upper bound, $P_s < 115$ atm. Comparable upper limits for a somewhat less realistic atmosphere were obtained by Jones (1964).

Some authors (Barrett 1961; Barrett and Staelin 1964; Thaddeus reported by Roman 1965) have attributed the declining brightness temperature of Venus in the millimeter-wave spectrum to pressure-induced transitions of CO_2 and N_2. We now see from the Mariner 2 results that the surface pressures on Venus are too low for this explanation to remain tenable. In addition, as we have mentioned, such models cannot explain the 8-mm phase effect.

From our upper limit on τ_s (19 mm, H_2O) we now estimate an upper bound on the Cytherean water-vapor abundance. The cross section per unit volume consists of two terms, κ_{res}, a resonant contribution, and κ_{nonres}, a nonresonant contribution. The opacity provided by the wings of the 13.5-mm water-vapor line account for κ_{res}; but at 19 mm, $\kappa_{nonres} \gg \kappa_{res}$. For example, at 10-atm pressure and an effective emitting temperature of 600°K, $\kappa_{nonres} = 4\kappa_{res}$. At higher pressures the nonresonant contribution dominates to an even greater extent, and in the following discussion we neglect κ_{res} entirely at 19 mm. The absorption coefficient is then given by

$$\kappa_{nonres} = 2.41\, \rho_{H_2O}\, \nu_G^2\, P\, T^{-2.125} \quad , \tag{48}$$

where ρ_{H_2O} is the density of water vapor in g/cm^3, P is the total pressure in atm, and T is the absolute temperature in °K (cf. Barrett and Staelin 1964).

We wish to relate τ (19 mm, H_2O) to w_{H_2O}, the total water vapor abundance in g/cm^2. Since $w_{H_2O} = \int \rho_{H_2O}\, dz$, the equation of state for a perfect gas, the approximation of a constant adiabatic lapse rate, Γ, and the Poisson relation yield, after integration,

$$w_{H_2O} = \frac{\mu_{H_2O}\, q_{H_2O}\, (\gamma - 1)}{\mathcal{R}\, \Gamma \gamma}\, P_s \quad ,$$

where μ_{H_2O} is the molecular weight of water, $\mathcal{R}$ is the universal gas constant, and γ is the ratio of specific heats, and is to be distinguished from the skin-depth ratio of equation (43). Analogously to our derivation of equation (46)

we can now explicitly integrate $\tau_s = \int \kappa_{nonres}\, dz$ for an adiabatic atmosphere in which water vapor is uniformly mixed (condensation near the top of this atmosphere will not significantly influence these results), finding

$$w_{H_2O} = 2.5 \times 10^3\, P_s^{-1}\, \tau(19\text{ mm},\ H_2O)\ , \qquad (50)$$

where w_{H_2O} is in g/cm^2 and P_s in atmospheres. The coefficient in equation (50) depends on the assumption $T_s = 700°\,K$; but since $w_{H_2O} \propto T_s^{2.125}$ variation in T_s by some tens of degrees will have little influence on our results.

To use equation (50) to establish an upper limit on w_{H_2O}, we must first have a lower limit on P_s. From two independent arguments--the CO_2 line broadening at 7820 Å (Spinrad 1962a), and the extension of dry adiabats from the 234° K clouds to the hot surface (Sagan 1962)--it follows that $P_s > 15$ atm. If τ_s (19 mm, H_2O) < 0.5, as the Mariner 2 data imply for surface depolarization, then equation (50) yields

$$w_{H_2O} < 85\ gm\ cm^{-2}\ ,\quad \epsilon\,(19\text{ mm}) = 1.45\ ; \qquad (51)$$

while if all the depolarization occurs in the atmosphere, so that τ_s (19 mm, H_2O) < 0.25,

$$w_{H_2O} < 45\ gm\ cm^{-2}\ ,\quad \epsilon\,(19\text{ mm}) = 3.6\ . \qquad (52)$$

If these upper limits of water vapor are uniformly mixed in atmospheres with surface pressures of some tens of atmospheres, we obtain upper limits to the water-vapor mixing ratio

$$q_{H_2O} \lesssim 10^{-3} \quad . \tag{53}$$

The observed mixing ratio in the vicinity of the Cytherean clouds is smaller than this upper limit by some two orders of magnitude (Bottema, Plummer, and Strong 1964; see also, Spinrad 1962b); but because of water condensation in the clouds it is possible that w_{H_2O} is as large as several tens of g/cm^2 above the surface of Venus (Sagan and Pollack 1966a).

Compared with the value $w_{H_2O} \sim 3 \times 10^5$ g/cm^2 for the terrestrial atmosphere and hydrosphere, the upper limits [equations (51) and (52)] point to a significant difference in water content between Earth and Venus that has planetary evolutionary implications. A model invoking preferential ultraviolet photodissociation of water vapor on Venus (effective because of large-scale reduction of the Cytherean surface preventing oxygen accumulation) and escape of hydrogen appears capable of accounting for the low relative water abundance on Venus (Sagan 1966).

VIII. SURFACE TEMPERATURE DISTRIBUTION AND THE SOURCES OF LIMB DARKENING IN THE SUCCESSFUL MODELS

a) Results on Surface Temperature Distributions

We now turn our attention to the successful models, the absorbing cloud and the distributed scatterers. For these models to reproduce the observations, a substantial longitudinal temperature gradient is required — as we have already qualitatively inferred from a preliminary examination of the Mariner 2 data. Our calculations of temperatures at the effective 19-mm radiating level (Table 4) predict that ΔT_g (b, t) > ΔT_g (d, t); such is not the case for the 40 percent depolarization entries of Table 5. We conclude that, while there may be some surface roughness depolarization, its magnitude must be less than 40 percent, in agreement with the results already extracted from the radar observations and several possible interpretations of the interferometric results. We have seen in the previous section that a secondary source of opacity, such as CO_2 or H_2O, may also lead to depolarization.

We can also estimate T_g (b) and T_g (d) from Table 5:

$$725^\circ \text{ K} \leq T_g \text{ (b)} \leq 835^\circ \text{ K},$$

$$635^\circ \text{ K} \leq T_g \text{ (d)} \leq 675^\circ \text{ K}.$$

That is, even without the qualitative requirement that ΔT_g (b, t) > ΔT_g (d, t), the Mariner 2 observations leads to an estimate of T_g (b) and T_g (d) in good agreement with the values computed (Table 4) from ground-based observations. If we further exclude the case of 40 percent depolorization, and require — as the ground-based observations suggest — that ΔT_g (t, b) > ΔT_g (t, d), then the lower limit on T_g (b) above becomes 760° K. The Mariner 2 observations

tend, therefore, to confirm the reality of the microwave phase effect reported at 3- and 10-cm wavelength. Note also that if we were to take the probable errors of Table 4 seriously, the value of T_g (b) would select from the last six entries of Table 5 the models with $\epsilon = 3.6$ over those with $\epsilon = 1.45$, and the absorbing cloud model over the distributed scatterer model. A better determination of the microwave phase effect at centimeter and decimeter wavelength would permit a more critical test of this conclusion.

The question of the surface temperature distribution and the choices among the surviving models in Table 5 will now be taken up in more detail. In our calculations of the temperatures at the effective emitting level for each scan, we derived dark- and bright-side temperatures separately; the use of $T_g = T_{g0} + T_{g1} \cos \eta$ [cf. eq. (43)], or some other simple representation of the longitudinal temperature dependence, was avoided because of our expectation of large latitudinal temperature gradients (Papers I and II; Clark and Kuz'min 1965). T_{g0} and T_{g1} are functions of latitude; errors as large as 50 K° in ΔT_g (t, d) are introduced if these coefficients are assumed constant.

Our present immediate objective is to obtain from the Mariner 2 data an estimate of T_1 (0, 0), the latitude-dependent coefficient of the time-variable term of the Venus surface temperature distribution [cf. eq. (38)]. We will, thereby, gain some insight into the factors determining T_g (b) and T_g (d), as well as estimating the longitudinal temperature gradient. Equation (43) exhibits the dependence through γ of T_g (19 mm) on the depth of the effective emitting layer. If the 19-mm emission arose from the surface itself, $\gamma = 1$ and $\psi = 0$ would obtain. For the actual depth of effective emission, our best estimates are $\gamma = 0.20$ and $\psi = 8.5°$ (cf. Paper II). With these choices, we may rewrite equation (43) as

$$T_g\,(19\text{ mm}) = T_0\,(0,\xi) + 0.83\,T_1\,(0,\xi)\cos\,[\eta + 8.5^\circ]. \qquad (54)$$

Two reasonable functional forms for each $T_0\,(0,\xi)$ and $T_1\,(0,\xi)$ in terms of $T_0\,(0,0)$ and $T_1\,(0,0)$, respectively, have been given in equations (39) to (42), with $a^{(i)} = a^{(ii)} = 0.30$.

We may obtain $T_0\,(0,0)$ from the condition that the first term of equation (54) multiplied by the emissivity e and integrated over the disk of Venus must be identically the brightness temperature of Venus, averaged over phase angles:

$$\int_{\varphi} e\,T_1\,(0,\xi)\,\frac{d\Omega}{\Omega} = \overline{T}_B \simeq 620^\circ\text{ K},\ 21\text{ cm} \geq \lambda \geq 3\text{ cm}. \qquad (55)$$

Using the coordinate transformation of Paper I and e = 0.89, we find $T_0^{(i)}\,(0,0) = 733^\circ$ K, and $T_0^{(ii)}\,(0,0) = 802^\circ$ K. With equation (40), we see that latitudinal effects can change $\Delta T_g\,(\underline{t},\underline{d})$ by 50 K° and $\Delta T_g\,(\underline{d},\underline{b})$ by 20 K°. With equation (39) the differences will be reduced substantially. Since the scan center of the dark-side scan is closer to the equator than either the terminator or bright-side scan centers (cf. Table 1), the first term in equation (54) will diminish $\Delta T_g\,(\underline{t},\underline{d})$ and $\Delta T_g\,(\underline{b},\underline{d})$, while the second term will tend to augment these differences slightly. In this regard, the first term proves to be dominant.

We now compute values of T_1 (0, 0) for three of the successful models of Table 5 — the 234° K absorbing cloud with an underlying surface dielectric constant ϵ of 3.6, and no surface depolarization; the same cloud with ϵ = 1.45; and the distributed scatterer with ϵ = 3.6 and no surface depolarization. In each case T_1 (0, 0) is computed separately in two ways, first from ΔT_g (t, b) and then from ΔT_g (t, d) through equation (54). The results of these calculations are exhibited in Table 6 for all combinations of the analytic form, equations (39) to (42), of the latitudinal temperature distribution. For comparison we also display values of T_1 (0, 0) for the same analytic forms, as derived from the phase-effect observations (Paper II).

TABLE 6

VALUES OF T_1 (0, 0) DERIVED FROM THE SUCCESSFUL MODELS OF THE MARINER 2 DATA

		Choice of Analytic Form			
		$T_0^{(i)}(0,\xi)$	$T_0^{(i)}(0,\xi)$	$T_0^{(ii)}(0,\xi)$	$T_0^{(ii)}(0,\xi)$
Model	Derivation	$T_1^{(i)}(0,\xi)$	$T_0^{(ii)}(0,\xi)$	$T_1^{(i)}(0,\xi)$	$T_1^{(ii)}(0,\xi)$
Absorbing cloud $\epsilon = 3.6$;0% depolarization	ΔT_g (b, t)	173° K	222	153	197
	ΔT_g (d, t)	58	62	129	140
Absorbing cloud $\epsilon = 1.45$	ΔT_g (b, t)	73	94	53	68
	ΔT_g (d, t)	125	135	197	212
Distributed scatterers $\epsilon = 3.6$	ΔT_g (b, t)	120	154	100	128
	ΔT_g (d, t)	66	71	137	148
From 3- and 10-cm phase effect		155	242	155	242

For the two $\epsilon = 3.6$ models, the results obtained from $\Delta T_g(\underline{b}, \underline{t})$ and $\Delta T_g(\underline{d}, \underline{t})$ are in reasonable agreement only for the analytic form $T_0^{(ii)}(0, \xi) = [1 - a^{(ii)} |\sin \xi|]\ T_1(0, 0)$, i.e., for a relatively steep latitudinal gradient of the time-dependent term of the temperature distribution. When we compare these surviving choices with the phase-effect results, we find that only the choice $[T_0^{(ii)}(0, \xi),\ T_1^{(i)}(0, \xi)]$ of analytic forms survives; however, the analytic forms chosen are merely representative, and any discrimination among the models from the precision of numerical agreement would be premature.

In the absorbing cloud model for $\epsilon = 1.45$, the values of $T_1(0, 0)$ derived from $\Delta T_g(\underline{b}, \underline{t})$ and from $\Delta T_g(\underline{d}, \underline{t})$ are in reasonable accord only for $T_0^{(i)}(0, \xi) = [1 - a^{(i)} + a^{(i)} \cos \xi]\ T_0(0, 0)$; i.e., for a more modest latitudinal gradient of the time-dependent term. Even in this case, the agreement with phase-effect results is not good, indicating a latitudinal temperature gradient somewhat shallower still. Note that, as discussed earlier in this section, consistent values of $T_1(0, 0)$ are obtained only when $|\Delta T_g(\underline{t}, \underline{b})| > |\Delta T_g(\underline{t}, \underline{d})|$.

Thus, while the observational uncertainties and the approximations utilized in this discussion introduce errors of several tens of degrees, many of the models have failed to pass the foregoing tests of internal consistency within the Mariner 2 data set, and others have failed when agreement was sought between the Mariner 2 and the ground-based observations.

b) Derived Values of τ (19 mm)

In Table 5 are displayed values of τ (19 mm) obtained from $T_{Bp}(\underline{t})$ of the second Mariner 2 scan. At first sight this procedure might seem unreliable since $T_{Bp}(t)$ is very close to the brightness temperature, about 620° K, observed at longer wavelengths where $\tau \simeq 0$; i.e., it might be claimed that the difference between $T_{Bp}(\underline{t})$ and 620° K is not significant and

that τ(19 mm) = 0 as well. Fortunately, a verification of this value of τ(19 mm) exists, viz., the value derived from 8-mm observations (cf. Table 3). The values of τ(19 mm) computed by these two different methods are in excellent agreement (cf. Tables 3 and 5) for all models, including the surviving absorbing cloud and distributed scatterer models.

We can also see qualitatively that reasonable variations in τ(19 mm) cannot alter our conclusions on which models survive. For the unsuccessful continuously distributed absorber models, the surface radiation must be significantly attenuated and the emissivity limb darkening greatly damped. Because of the strong dependence of τ on T_s, these models must predict a small limb darkening, contrary to observation. For the successful absorbing cloud and distributed scatterer models with $\epsilon = 3.6$, τ is smaller and the observed limb darkening due almost entirely to the dependence of emissivity on μ. Small variation in τ will leave the predictions for these models unaltered. For these models with $\epsilon = 1.45$, the limb darkening is primarily due to τ/μ, and so the numerical value of τ has an important influence on the limb darkening. However, $eT_s \simeq 690°$ K for $\epsilon = 1.45$; thus, the differences between eT_s and $T_{Bp}(\underline{t})$ are significant beyond the observational errors.

Consequently we can conclude with some safety that if ϵ(19 mm) $\simeq$ 3.6, then $\tau \propto \lambda^{-2}$ is a good approximation for 8 mm $\leq \lambda \leq$ 2 cm; while if ϵ(19 mm) $\simeq$ 1.45, $\tau \propto \lambda^{-1}$ is appropriate over the same range.

c) Summary of the Limb-Darkening Physics and Parameter-Dependence of the Models

We now summarize the physical basis of limb darkening in the foregoing models, and discuss the dependence of the predicted limb effects on the parameters assumed or deduced. For models in which an absorber is continuously distributed throughout the atmosphere, the limb darkening is primarily due to τ/μ. Because the optical depth is sizable in these models--e.g., $\tau/\mu \simeq 1.5$ for the center of the d scan and $\simeq 2$ for the center of the b scan for CO_2--the

influence of surface emissivity on the observed limb darkening is small. Despite the large attenuation of the surface emission by the atmosphere in these models, the radiation emitted to space arises from very near the surface and variations in τ will have small effect on the limb darkening. Further, τ depends very sensitively on T_s; thus, the temperature of the effective emitting layer varies little with a change in μ. For the reason already mentioned, and as illustrated for the $\epsilon = 1.45$ and $\epsilon = 3.6$ cases (Table 5), these continuously distributed absorber models depend very little on the surface dielectric constant.

While CO_2-N_2 mixtures and water vapor are excluded as general sources of opacity, because of the strong dependence of τ_s on T_s, composite models in which these absorbers make noticeable contributions on the dark side are not excluded; in particular, there may be an influence of such absorbers on the opacity of the subterrestrial point observed at inferior conjunction by 3-cm radar (cf. Paper II). Such an effect would only slightly modify the results of the present paper.

The foregoing calculations were carried out assuming an adiabatic lapse rate, which we expect on the basis of an application of the Schwarzschild instability critierion to Venus. If, however, we were to alter the temperature gradient uniformly at all positions on the surface, the effect for these models will be negligible (cf. the $s = 0$ and $s = 0.4$ entries for absorbing dust in Table 5). Even varying τ_s across the disk of Venus in the absorbing dust case will have no major consequences for the limb darkening, provided the variation lies within the constraints imposed by the 8-mm phase effect.

With the absorbing-cloud case we encounter the virtue of an opacity source at temperatures substantially below the surface temperature. In the distributed scatterer model there is no reradiation, and in this context, its effective temperature vanishes. Accordingly, in both these models, τ(19 mm) can be small for $\epsilon = 3.6$, and the emissivity limb darkening can dominate. When $\epsilon = 1.45$ in the absorbing-cloud model, τ becomes sufficiently large

that both τ/μ and $e(\mu)$ are important for the limb darkening. Again, the fact that $T_c \ll T_s$ permits substantial emissivity limb darkening. Note that inequalities (35) and (36) place severe constraints on the possibility that a variation of τ with position on Venus can influence the results for these two models. For example, with $\epsilon = 3.6$ in the absorbing cloud model, the maximum allowable variation of τ changes $\Delta T_{Bp}(\underline{d}, \underline{b})$ by 15 K^o.

IX. PARTICLE SIZES IN THE CLOUD AND SCATTERER MODELS

We now consider the successful models from a more general viewpoint, further examining their consistency and other implications. Both successful models, the absorbing cloud and the distributed scatterers, invoke extinction by liquid or solid particles, rather than absorption by molecules in the gas phase. A useful parameter for describing absorption and scattering by a spherical particle is $x = 2\pi a/\lambda$, where a is the particle radius and λ the wavelength of incident light. In the following discussion we will assume spherical particles. As x declines below unity, the scattering cross-section Q_s falls off much more rapidly than the absorption cross-section Q_a. Over the stated range in x for ice and dust particles at microwave frequencies, Q_s and Q_a are given to better than 10 per cent accuracy by the following expressions:

$$Q_s \simeq \frac{8}{3}\pi a^2 x^4 \left| \frac{\epsilon_c - 1}{\epsilon_c + 2} \right|^2 , \qquad x < 1.0 \tag{56}$$

and

$$Q_a \simeq 4\pi a^2 x \, \mathrm{Im}\left\{ \frac{\epsilon_c + 1}{\epsilon_c - 2} \right\} , \qquad x < 0.4 \tag{57}$$

(van de Hulst 1957), where ϵ_c is the complex dielectric constant of the particle and equals $\epsilon_r - \sqrt{-1}\,\epsilon_i$. The quantities ϵ_c, ϵ_r, and ϵ_i for the particles are to be distinguished from ϵ, the real part of the Cytherean surface dielectric constant, discussed in previous sections. In the common case that $\epsilon_i \ll \epsilon_r$, equation (57) reduces to

$$Q_a \cong 4\pi a^2 x \frac{\epsilon_i}{\epsilon_r + 2} , \qquad x < 0.4 \tag{58}$$

Relations (56) and (57) also apply to liquid water at microwave wavelengths when $x < 0.1$.

We now define x_{crit} as the value of x when $Q_s = Q_a$. Because Q_s declines much faster with a decrease in x than does Q_a, when $x < x_{crit}$, the extinction of the radiation will be due almost entirely to pure absorption. If $\epsilon_i \ll \epsilon_r$, then

$$x_{crit}^3 \simeq 4.5\,\epsilon_i(\epsilon_r - 1)^{-2}\,. \tag{59}$$

For dust at microwave frequencies, ϵ_r is generally about 3– although for some materials it may range as high as 10 – and ϵ_i varies from 10^{-3} to 10^{-1}, depending on the composition and impurity content (see Paper II). For ice at microwave frequencies and the temperatures of interest, $\epsilon_i \sim 10^{-3}$. Using equation (59) to obtain x_{crit}, with λ = 19 mm, we can find a_{max}, the maximum size of a particle of given composition for which absorption dominates, and scattering can be neglected. Values of x_{crit} and a_{max} are given for dust, ice, and liquid water, and for λ = 19 mm, in Table 7. Equations (56) and (57) were used directly for the liquid water calculations since ϵ_i is comparable to ϵ_r.

TABLE 7

PARTICLE PROPERTIES IN THE ABSORBING CLOUD AND DISTRIBUTED SCATTERER MODELS

Substance	x_{crit}	a_{max} (mm)	x^*	v_t (miles/hr)
Liquid water	~0.3	0.9	1	13.
Ice	0.1	0.3	2	3.1
Dust, $\epsilon_i = 10^{-3}$	0.1	0.3	2	9.3
Dust, $\epsilon_i = 10^{-2}$	0.2	0.6	2	33.
Dust, $\epsilon_i = 10^{-1}$	0.5	1.5	2	57.

When $x > x_{crit}$, scattering will dominate for all $x > x_{crit}$ for liquid water droplets and at least to very high values of x for ice and dust – a statement we now undertake to justify. For these values of x, radiation may be diffracted around the particle, reflected at the surface of the particle, or transmitted through the particle. Of the radiation either reflected or transmitted, an estimate of the fraction of radiation reflected can be obtained from the appropriate Fresnel power equation at normal incidence,

$$R(0, \lambda) = \left| \frac{\epsilon_c^{1/2} - 1}{\epsilon_c^{1/2} + 1} \right|^2 . \qquad (60)$$

This equation is valid in or near the geometric domain out to very oblique angles, and gives a fair representation of the reflectivity for particles of a variety of shapes.

For liquid water at 19 mm, $R(0, \lambda)$ is very close to unity, and water droplets behave metallically at these frequencies. Thus, for $x > x_{crit}$, Q_s will dominate the extinction cross section for water. For dust and ice, $R(0, \lambda) \sim 0.1$; thus, the absorptivity is given approximately by $\exp(-2xn') = \exp(-\epsilon_i x/\epsilon_r)$, where n' is the imaginary part of the index of refraction (see van de Hulst 1957). Since $\epsilon_i \ll \epsilon_r$ for ice and dust, once $x > x_{crit}$, absorption is important only for very large values of x. Thus for water droplets, for ice, and for dust, absorption dominates when $a < a_{max}$, and scattering dominates when $a > a_{max}$. Hence, the absorbing cloud model and the distributed scattering model can be distinguished by the mean particle size responsible for attenuation.

With the aid of equation (58) we can obtain the wavelength dependence of the optical depth for the absorbing-cloud model. Unlike the case for liquid water, ϵ_r and ϵ_i for ice and dust exhibit little wavelength dependence at microwave frequencies; for these substances $\tau \propto \lambda^{-1}$ approximately (see, e.g., Paper II), provided $x < x_{crit}$ at the wavelengths of interest. From Tables 5 and 3 we see that ϵ (19 mm) $\simeq 1.45$ implies $\tau \propto \lambda^{-1}$, more closely than $\tau \propto \lambda^{-2}$. It is important, therefore, to examine more closely the $\tau(\lambda)$ dependence of Venus and of liquid water droplets and determine whether water droplet clouds are excluded should ϵ (19 mm) prove to be 1.45.

We will assume $\tau \propto \lambda^{-q}$ and determine q as carefully as we can, first from observations of Venus, and then from laboratory measurements on water. As detailed above, τ (19 mm) can be estimated with a fair degree of confidence, directly from the Mariner 2 data when ϵ (19 mm) = 1.45, since

$T_B(\underline{t})$ will then be significantly below the brightness temperature of the ground. A lower bound to τ(19 mm) is obtained from the requirement that $\Delta T_g(\underline{b}, \underline{t}) > \Delta T_g(\underline{t}, \underline{d})$. An upper bound is obtained from the requirement that $T_B(\underline{t})$ agree within the probable error with the Mariner 2 temperatures. Thus, we find

$$0.20 \leq \tau(19 \text{ mm}) \leq 0.35 \quad . \tag{61}$$

To determine q, τ(19 mm) must be compared with τ(8 mm). If we take the phase-averaged 8-mm brightness temperature of Venus as 425°K (Basharinov et al. 1964) and allow for the usual absolute calibration errors, we find 470°K as an upper bound for this quantity, and 0.45 as a lower bound on τ(8 mm)--derived from the brightness temperatures at longer wavelengths. With the same errors, we find 385°K as a lower bound on $\overline{T}_B$(8 mm). The actual phase-averaged 8-mm brightness temperature is much more likely to lie near the smaller of these extremes; e.g., Tolbert and Straiton (1964) quote an 8.6-mm brightness temperature near inferior conjunction of 375 ± 52°K, and Copeland and Tyler (1964) report 353 ± 10°K. Adopting 385°K as a conservative lower bound on $\overline{T}_B$(8 mm), we find that the upper bound on τ(8 mm) depends on the temperature, T_c, of the absorber in the clouds. Thus,

$$\left.\begin{aligned} 0.45 \leq \tau(8\,\text{mm}) \leq 0.80 \quad , \quad T_c = 253°\text{K} \\ 0.45 \leq \tau(8\,\text{mm}) \leq 1.00 \quad , \quad T_c = 293°\text{K} \end{aligned}\right\} \quad . \tag{62}$$

From (61) and (62) we find

$$\left.\begin{aligned} 0.3 \leq q \leq 1.6 \quad , \quad T_c = 253°\text{K} \\ 0.3 \leq q \leq 1.9 \quad , \quad T_c = 293°\text{K} \end{aligned}\right\} \quad . \tag{63}$$

Considering the alternative 8-mm brightness temperature measurements, it seems safe to conclude that q lies between 1 and 2, with perhaps somewhat more likelihood that it lies nearer the smaller value if $\epsilon(19\,\text{mm}) \simeq 1.45$. This confirms the less-detailed conclusions drawn from Tables 3 and 5.

We now estimate q for liquid water droplets. The problem is characterized by the Debye wavelength λ_D for hindered rotation of water molecules. For $\lambda \gg \lambda_D$, q = 2. However, at the wavelength region of interest $\lambda \sim \lambda_D$ and q must be computed from the general Debye equations. Further, λ_D depends sensitively on temperature; because of increasing viscosity of water with decreasing temperatures, λ_D increases as the temperature drops. The dependence of τ on λ is given by (see, e.g., Basharinov and Kutuza 1965)

$$\tau(\lambda) \propto \frac{1}{\lambda} \frac{\epsilon_i}{(\epsilon_r + 2)^2 + \epsilon_i^2} \quad , \tag{64}$$

where ϵ_r and ϵ_i, respectively the real and imaginary parts of the dielectric constant of water, are

$$\epsilon_r = \epsilon_\infty + \frac{\epsilon_0 - \epsilon_\infty}{1 + (\lambda_D/\lambda)^2} \tag{65}$$

and

$$\epsilon_i = \frac{\epsilon_0 - \epsilon_\infty}{1 + (\lambda_D/\lambda)^2} \frac{\lambda_D}{\lambda} \quad . \tag{66}$$

Basharinov and Kutuza give approximate values of λ_D and ϵ_0 for various temperatures of interest; $\epsilon_\infty \simeq 5$, and is apparently independent of the temperature (Hasted 1961). With this information we find

$$\left.\begin{array}{ll} q = 1.7 \pm 0.2 \quad , & T_c = 253°K \\ q = 2.0 \pm 0.1 \quad , & T_c = 293°K \end{array}\right\} \quad , \tag{67}$$

where the probable errors are our rough estimates. Thus, we find that the observed value of q for Venus between 8 and 19 mm when the surface dielectric constant at 19 mm is 1.45 is not inconsistent with liquid water clouds. While the results of equations (63) and (67) show an overlap only in a small part of the range in q, other acceptable choices for $\overline{T}_B$ (8 mm) would have greatly improved the fit. This crude agreement is important because should ϵ (19 mm) prove to be 1.45, of all the models in the present paper only the absorbing water cloud will have survived.

For a variety of reasons attenuation of millimeter waves by absorbing clouds of ice or dust is unlikely. At the temperatures prevailing at the Cytherean clouds, both ice crystals and water droplets should be present if there is condensed water at all. Since ϵ_i is a factor $\sim 10^3$ larger for liquid water than for ice, it is very unlikely that the microwave opacity in the absorbing-cloud model is due principally to ice. As for dust there is an immediate difficulty concerning why it should be localized in a cloud layer, rather than continuously distributed throughout the atmosphere; this difficulty may not be insuperable, however (see Sagan and Kellogg 1963). Absorbing dust clouds require a very large amount of dust, since ϵ_i is very small. Moreover, the visible and near-infrared reflection spectrum of Venus is consistent with scattering from ice crystals, with liquid water droplets below, and is probably inconsistent with all form of dust (Sagan and Pollack 1966b). Thus, should the millimeter opacity be due to absorbing clouds, rather than to scattering, water droplets in the clouds are the most likely explanation.

We now consider the wavelength dependence of optical depth for the scattering model. For dust and ice, the total extinction coefficient reaches an approximately constant value when $x > 2$; the corresponding value for liquid water is $x > 1$ (e.g., van de Hulst 1957). We denote these values of x by x*. While for a given particle size, and for large x, Q_{ext} tends to oscillate, a particle size distribution will tend to damp the oscillations; thus when x, defined for the mean particle size, exceeds x*, Q_{ext} will remain approximately constant. The observed brightness temperature of Venus declines steadily from $\lambda = 3$ cm to $\lambda = 3$ mm. Values at submillimeter wavelength are not available at the present time, but a continuing decline can be inferred by the neccessity that brightness temperatures join smoothly with the infrared radiometric temperatures $\sim 230^{\circ}$K. Thus the scattering model requires that the largest value of x at 3-mm wavelength be x*; on the other hand this model also requires that x exceed x_{crit} at 19 mm. Thus the constraints on the scattering model are

$$\left.\begin{aligned} &x(\lambda = 3 \text{ mm}) < x^* \\ &x(\lambda = 19 \text{ mm}) > x_{crit} \end{aligned}\right\} . \tag{68}$$

Comparing these constraints with the values of x_{crit} and x* given in Table 6, we find that they are compatible only with a very small range in particle size, centered about $a \simeq 0.5$ mm. Similar particle sizes were derived by Barrett and Staelin (1964) in an attempt to match the microwave spectrum with a continuous distribution of dust in the Cytherean atmosphere; and it was earlier recognized by Öpik (1961) that particle radii roughly in this size range are required for effective microwave extinction by nonabsorbing dust. This assignment of particle size justifies our previous assumption of isotropic scattering, since $x(19\text{mm}) \simeq 0.3$ (cf., Penndorf 1956).

The scattering model makes no demands on the distribution of scattering centers in the Cytherean atmosphere; they may be localized in a cloud layer, or continuously distributed through the atmosphere. Let us consider the possible identification of the scattering layer with the clouds. The polarization phase dependence of Venus suggests that the particles in the upper clouds have radii $\simeq 2 \times 10^{-3}$ mm (Lyot 1929; van de Hulst 1952), several orders of magnitude smaller than the sizes deduced here. While some mass segregation with altitude can be expected, it is an open question whether a segregation of this order is plausible. Secondly, because of their large radii, 0.5-mm scattering particles must possess large terminal velocities. This point is illustrated in Table 6, where deviations from Stokes' law at large particle radii (e.g., Gunn and Kinzer 1949, Ryan 1964), and the viscosity of air at S.T.P. are assumed.

If the microwave attenuation is attributed to scattering dust particles in the visible clouds, then Cytherean winds must very efficiently transport large particles to high altitudes to replenish the supply lost by falling. We must also imagine that these particles are somehow prevented from reaching the lower atmosphere. If the scatterers or absorbers are in the clouds and are composed of water, then large raindroplets or small hailstones must be continuously generated in great numbers in the clouds to replace those falling to lower altitudes and there vaporized. We do not know whether the required generation rate of large condensates is meteorologically plausible. If there is a major contribution from scattering to the millimeter opacity, the most likely models appear to be a cloud of falling raindrops and hailstones, or a continuous vertical distribution of dust from the cloud drops to the surface. Similar models have been suggested by Deirmendjian (1964) and by Öpik (1961), respectively. However, because of the almost unique restriction on particle size which these models require (cf. eq. (68)), and the inability of these models to explain the visible and near-infrared albedo (Sagan and Pollack 1966b), we believe that an absorbing-cloud composed of smaller ice crystals and water droplets is in better agreement with the observations taken as a whole. Further discussion of the case for water clouds on Venus can be found in Sagan and Pollack (1966a, b).

Future studies of 3-cm radar scattering from Venus can make possible a much clearer choice among the models. Note that the effective subsurface depth examined by radar at 3.6 cm is approximately that seen by passive observations at 19 mm. The radar beam twice traverses the immediate subsurface layers, and so reaches a depth only about half as great as that from which emission of the same wavelength occurs. Further, $z_e \sim \lambda$. If ϵ (19 mm) proves to be about 1.45, all scattering models are excluded, because the unacceptable condition $\Delta T_g(\underline{b}, \underline{t}) < \Delta T_g(\underline{t}, \underline{d})$ would then apply. Moreover, for this surface dielectric constant, an absorbing cloud can be made to fit the limb darkening through the factor $\exp[-\tau/\mu]$. But the scattering models depart from an $\exp[-\tau/\mu]$ dependence for anything but small τ/μ because of multiple scattering, which tends to reduce the limb darkening.

Thus, if $\epsilon(19\,\text{mm}) \simeq 1.45$, scattering models are excluded, and of the absorbing cloud models, only liquid water clouds are consistent with the observations. For larger values, $1.45 < \epsilon(19\,\text{mm}) \leq 3.6$, water clouds are still the preferred model, but not as rigorously as when $\epsilon(19\,\text{mm}) \simeq 1.45$.

X. CONCLUSIONS

This paper has investigated the internal consistency, and the agreement with ground-based observations, of a variety of models of the 19-mm Mariner 2 limb-darkening measurements. We have found that water vapor, CO_2-N_2 mixtures at elevated pressures, and absorbing dust as opacity sources are incompatible with the Mariner 2 observations, while agreement can be secured by either an absorbing-cloud layer (composed, e.g., of water droplets, of ice crystals, or of dust) or a scattering aerosol arbitrarily distributed with altitude. A discriminant against the successful models is provided by the value of the surface dielectric constant, as determined by 3.6-cm radar observations. If $\epsilon(19\,\text{mm}) \simeq 1.45$, then only the absorbing cloud survives, and an opacity due to water droplets is strongly indicated over the other alternatives. But if $\epsilon(19\,\text{mm}) \simeq 3.6$, then all the previously successful models remain; from other evidence, absorbing water droplet clouds, and distributed scatterers are the most likely models. In the scattering models, the particle radii must be close to 0.5 mm. Dust scattered throughout the atmosphere is the most likely opacity source due to scattering; but hailstones or large water droplets formed in the clouds are possible alternatives.

The Mariner 2 observations yield a large temperature difference—between 100 and 150 K°--between the equatorial terminator and the subsolar point. A similar difference holds between the equatorial terminator and the anti-solar point. These longitudinal temperature gradients are in good agreement with those deduced from the microwave phase effect (Paper II). The exclusion of the CO_2-N_2 and the water vapor models has provided useful upper limits on the surface pressure, P_s, and the total water vapor content, w_{H_2O}, of the atmosphere. We have found P_s less than 115 to 150 atm--depending on the CO_2 mixing ratio; further, $w_{H_2O} < 85$ g cm^{-2} for $\epsilon(19\,\text{mm}) = 1.45$, and $w_{H_2O} < 45$ g cm^{-2} for $\epsilon(19\,\text{mm}) = 3.6$.

We now comment briefly on the theoretical discussion of the Mariner 2 data in the thesis of Jones (1964). This paper was made available to us, after the principal results of the present paper were secured, through the courtesy of Dr. Jones. His discussion considers only the case ϵ (19 mm) $\simeq$ 3.6. In agreement with the 8- to 13-μ radiometric observations, and evidence that the temperature range through the clouds is only a few tens of degrees, we have assumed an isothermal cloud at T_c = 234° K. Jones found that absorbing clouds at $T_c \leq 350°$ K match the 19-mm observations satisfactorily. It is clear from our previous discussion that as long as $T_c \ll T_s$ agreement with the Mariner 2 limb-darkening observations can be secured. Jones prefers 350° K clouds primarily for three reasons: 1) the apparent bi-modal Boltzmann distribution of the rotational lines of the 7820 A CO_2 band, pointed out by Kaplan (1963) and based on the ground-based observations of Spinrad (1962a); 2) the apparent difficulty in fitting both 4-mm and 8-mm ground-based brightness temperatures with liquid water clouds at $T_c \sim 234°$ K; and 3) the difficulty in accounting with 230° K clouds for the apparent absence of limb darkening at 13.5 mm as observed by Mariner 2. A cloud at T_c = 350° K cannot be made of water; Kaplan suggested hydrocarbons, some of which condense at 350° K, and all of which absorb at 3.5μ, an apparent window in the CO_2, N_2, and H_2O atmosphere of Venus, which must be filled for successful greenhouse models of the high-surface temperature to be constructed. However, thermodynamic equilibrium studies show hydrocarbons and other organic molecules to be extremely unstable in the Cytherean atmosphere (Lippincott, Eck, Dayhoff, and Sagan 1966); the radar observations are inconsistent with large quantities of surface hydrocarbons (Paper II); and the 3.5-μ window is very effectively plugged either by condensed or by vapor phase water (Sagan and Pollack 1966a). Further, some skepticism has been expressed (Spinrad 1965) about the reality of the J-number double maximum, and, in any case, no solution of this line-formation problem in the Venus atmosphere has been published.

The apparent difficulty in matching 4-mm and 8-mm observations simultaneously with liquid water clouds has been noticed by several workers (Sagan and Giver 1961; Rasool 1963; Salomanovich 1964; Barrett and Staelin 1964). However Basharinov and Kutuza (1965) have recently shown that the absorption properties of super-cooled water are different from those

of water above 0° C, and can account for the millimeter spectrum. In addition, a strightforward analysis of the visible and near infrared albedo of Venus leads to ice-crystal clouds with ~ 0.1 g/cm^2 of super-cooled water droplets below (Sagan and Pollack, 1966a, 1966b). This abundance of liquid water is just the amount required to account for the general shape of the millimeter spectrum of Venus. We prefer to treat with some caution any conclusion drawn from the 13.5-mm channel, which was characterized by low signal-to-noise and an erratic baseline. Accordingly, we conclude that 234° K absorbing water clouds are much more strongly indicated than 350° K absorbing clouds of some unspecified carbonaceous material. Jones also concluded that the pressure-induced CO_2 - N_2 model and the water vapor model do not satisfy the Mariner 2 observations, a conclusion he verified for a range of values of the optical depth.

Future microwave observations of Venus from flyby or orbiter spacecraft are clearly desirable. Measurements made with high-topographical resolution will permit a much better specification to be made of the nature and three-dimensional distribution of microwave attenuators, and of the surface temperature distribution. High-resolution millimeter measurements near the antisolar point and the rotational poles will permit a check on the influence of CO_2 - N_2 mixtures and water vapor — materials that increase in opacity with decreasing temperatures — on the overall optical depth. Infrared searches for water vapor may acquire most of their photons from the vicinity of the clouds. In contrast an operating 13.5-mm experiment with high signal-to-noise, and with adjacent channels at nearby wavelengths to test line shape, is the most effective method of investigating the presence of water vapor on Venus, and determining its distribution and total abundance above the surface.

Acknowledgments

This research was supported in part by an award from the Alfred P. Sloan Foundation and by Grant NGR-09-015-023 from the National Aeronautics and Space Administration. We are particularly indebted to Mariner 2 microwave Experimenter Dr. D. E. Jones of the Jet Propulsion Laboratory and Brigham Young University for a generous and detailed discussion of the instrumentation, observational errors, and data reduction. We also gratefully acknowledge a fruitful discussion with Experimenter Prof. A. E. Lilley of Harvard College Observatory. It is a pleasure to thank Mrs. Elinore Green and Mrs. Andrea Dupree for assistance, with desk and electronic computers, with the calculations.

REFERENCES

Barath, F. T., Barrett, A. H., Copeland, J., Jones, D. E., and Lilley, A. E. 1964, Astron. J., 69, 49.

Barrett, A. H. 1961, Ap. J., 133, 281.

_____. 1965, Radio Science, 69D, 1565.

Barrett, A. H., and Staelin, D. H. 1964, Space Sci. Revs., 3, 109.

Basharinov, A. E., Vetukhnovskaya, Y. N., Kuz'min, A. D., Kutuza, B. G. and Salomonovich, A. E. 1964, Astron. Zh., 41, 707.

Basharinov, A. E., and Kutuza, B. G. 1965, Radio Science, 69D, 1580.

Bottema, M., Plummer, W., and Strong, J. 1964, Ap. J., 139, 1021.

Carpenter, R. L. 1964, Astron. J., 69, 2.

_____. 1966, Science, in press.

Chamberlain, J. W. 1965, Ap. J., 141, 1184.

Chandrasekhar, S. 1950, Radiative Transfer (Oxford: Clarendon Press).

Chandrasekhar, S., and Elbert, D. 1952, Ap. J., 115, 269.

Clark, B. G., and Kuz'min, A. D. 1965, Ap. J., 142, 23.

Copeland, J., and Tyler, W. C. 1964, Ap. J., 139, 409.

Deirmendjian, D. 1964, Icarus, 3, 109.

Gibson, J. E., and Corbett, H. H. 1963, Astron. J., 68, 74.

Gunn, R., and Kinzer, G. D. 1949, J. Meteorol., 6, 243.

Hasted, J. B. 1961, Progress in Dielectrics (J. B. Birks and J. Hart, eds.), vol. 3 (New York: Wiley and Sons).

Ho, W., Osborn, R., and Thaddeus, P. 1963, Columbia Radiation Lab., Fourth Quarterly Progr. Rept., 58.

Jones, D. E. 1964, Thesis, Brigham Young University.

_____. 1965, private communication.

Kaplan, L. D. 1963, J. Quant. Spectros. Radiat. Transfer, 3, 537.

Karp, D., Morrow, W. E., Jr., and Smith, W. B. 1964, Icarus, 3, 473.

Lippincott, E. R., Eck, R. V., Dayhoff, M. O., and Sagan, C. 1966, to be published.

Lyot, B. 1929, Ann. Obs. Paris (Meudon), 8, 1.

Murray, B. C., Wildey, R. L., and Westphal, J. A. 1963, J. Geophys. Res., 68, 4813.

Opik, E. J. 1961, J. Geophys. Res., 66, 2807.

Penndorf, R. 1956, Geophysical Research Paper No. 45 (Cambridge Air Force Research Center).

Pollack, J. B., and Sagan, C. 1965a, Ap. J., 141, 1161 [Paper I].

_____. 1965b, Icarus, 4, 62 [Paper II].

_____. 1965c, J. Geophys. Res., 70, 4403.

Rasool, S. I. 1963., Proc. XIth Intern. Astrophys. Symp., Liège, Belgium, 1962, 367.

Roman, N. G. 1965, Astron. J., 70, 630.

Ryan, J. A. 1964, J. Geophys. Res., 69, 3759.

Sagan, C. 1962, Icarus, 1, 151.

_____. 1966, International Dictionary of Geophysics (S. K. Runcorn, Editor-in-chief) (London: Pergamon Press).

Sagan, C., and Giver, L. 1961, Paper delivered at Am. Geophys. Union Symp. on Radio Emission and Thermal Structure of the Venus Atmosphere. U. C. L. A. Also: Rept. NASA Grant NsG-126-61.

Sagan, C., and Kellogg, W. W. 1963, Ann. Rev. Astron. Astrophys., 1, 235.

Sagan, C., and Pollack, J. B. 1966a, to be published.

_____. 1966b, Proc. Caltech-JPL Lunar and Planetary Conf. (H. Brown et al., eds.) in press.

Salomonovich, A. E. 1964, Life Sciences and Space Research (Florkin, M. and Dollfus, A., eds.) (Amsterdam: North-Holland Publ. Co.), Vol. 2.

Scarf, F. L. 1963, J. Geophys. Res., 68, 141.

Sinton, W. M., and Strong, J. 1960, Ap. J., 131, 470.

Spinrad, H. 1962a, Publ. Astron. Soc. Pacific, 74, 187.

_____. 1962b, Icarus, 1, 266

_____. 1965, private communication.

Thaddeus, P. 1965, private communication.

Tolbert, C. W., and Straiton, A. W. 1962, J. Geophys. Res., 67, 1741.

_____. 1964, Nature, 204, 1242.

van de Hulst, H. C. 1952, The Atmospheres of the Earth and Planets (G. P. Kuiper, ed.) (Chicago: University of Chicago Press), Chap. 3.

_____. 1957, Light Scattering by Small Particles (New York: Wiley and Sons).

Walker, R., and Sagan, C. 1966, Icarus, 5, in press.

Welch, W. J., and Thornton, D. D. 1965, Astron. J., 70, 149

PROPERTIES OF THE CLOUDS OF VENUS

Carl Sagan

Harvard University
and
Smithsonian Astrophysical Observatory
Cambridge, Massachusetts

James B. Pollack

Smithsonian Astrophysical Observatory
Cambridge, Massachusetts

ABSTRACT

We have obtained in the Schuster-Schwarzschild approximation theoretical formulae describing the monochromatic transmissivity, reflectivity, and absorptivity of a cloud layer characterized by an arbitrary single scattering albedo and anisotropic phase function. The application of this formalism combined with exact solutions to the Mie theory problem to the observed visual and near infrared reflectivity of Venus permits the determination of a number of properties of the Cytherean cloud layer. We confirm Strong's identification of ice as the principal constituent of the clouds. In addition the mean radius of cloud particles lies between 7.5 μ and 10 μ, while the interaction optical depth of the layer is between 18 and 43. Clouds with these properties allow a sizable fraction of the incident sunlight to penetrate to the surface, but are extremely opaque to radiation thermally produced by the planet. A greenhouse mechanism therefore appears to be operative which can explain the high surface temperature of Venus.

The reflection spectra obtained from dispersed media--both clouds and powders--depend on the monochromatic single scattering albedo, the single scattering phase function, the particle size distribution, the total optical depth, and the albedo of the underlying surface. A successful analysis of observed spectra should extract most of the foregoing parameters from the observations. We now describe a method for calculating the fraction of monochromatic radiation reflected, transmitted and absorbed by a layer of dispersed particles having arbitrary characteristics; and then apply the method to an examination of the clouds of Venus.

For wavelengths at which the cloud particles are large compared with the wavelength, the particles may scatter a very large fraction of the radiation into the forward hemisphere; in this case isotropic scattering is a poor assumption. For expected particle sizes of dust grains, ice crystals, or water droplets anisotropic scattering will be important in the visible and near infrared. The appropriate equation of radiative transfer for monochromatic radiation nonconservatively and anisotropically scattered by a dispersed medium is

$$\mu \frac{dI}{d\tau} = - I + \int_{\Omega'} I \, p \, \frac{d\Omega'}{4\pi} \qquad (1)$$

where I is the specific intensity, τ the optical depth, Ω' the solid angle, arc cos μ the angle between the direction of propagation and the local planetary normal, and p the scattering phase function (cf., e.g., Chandrasekhar, 1950); the integration is over all solid angles. Eq. (1) may be re-written in the Schuster-Schwarzschild, or two-stream, approximation as

$$3^{-1/2} \frac{dI_+}{d\tau} = -I_+ + I_+ \tilde{\omega}_0 (1 - \beta) + I_- \tilde{\omega}_0 \beta$$

$$- 3^{-1/2} \frac{dI_-}{d\tau} = - I_- + I_- \tilde{\omega}_0 (1 - \beta) + I_+ \tilde{\omega}_0 \beta \qquad (2)$$

where I_+ is the average specific intensity in the $+d\tau$ hemisphere, and I_- is the average specific intensity in the $-d\tau$ hemisphere. β is a measure of the fraction of radiation singly scattered into the backward hemisphere of the incident radiation. It equals 1/2 for isotropic scattering, and about 1/15 for ice crystals $\sim 10\ \mu$ in radius and visible radiation; β is related to other scattering parameters below. Note in eqs. (2) that the backward hemisphere for I_+ is in the $-d\tau$ direction, but in the $+d\tau$ direction for I_-. The factor $3^{-1/2}$ in eqs. (2) represents the appropriate average value of μ in the two-stream approximation (Chandrasekhar, 1950).

Equations (2) are two coupled linear first order differential equations with constant coefficients, and may be solved in closed form by well-known techniques. Let $\mathcal{A}$, $\mathcal{R}$, and $\mathcal{T}$ be, respectively, the fraction of the incident radiation absorbed, reflected, and transmitted by the dispersing medium. For the boundary condition of negligible surface albedo, the solution of eqs. (2) is

$$\mathcal{R} = \frac{(u+1)(u-1)\left[\exp(\tau_{eff}) - \exp(-\tau_{eff})\right]}{(u+1)^2 \exp(\tau_{eff}) - (u-1)^2 \exp(-\tau_{eff})} \tag{3}$$

$$\mathcal{T} = \frac{4u}{(u+1)^2 \exp(\tau_{eff}) - (u-1)^2 \exp(-\tau_{eff})} \tag{4}$$

$$\mathcal{A} = 1 - \mathcal{R} - \mathcal{T} \tag{5}$$

where

$$u^2 = \frac{1 - \tilde{\omega}_0 + 2\beta\ \tilde{\omega}_0}{1 - \tilde{\omega}_0} \tag{6}$$

and

$$\tau_{eff} = 3^{1/2}\ u(1 - \tilde{\omega}_0)\ \tau_1 \tag{7}$$

In eq. (7), τ_1 is the total interaction optical depth of the clouds; i.e., $\exp(-\tau_1)$ represents the fraction of the incident radiation which experiences neither absorption nor scattering during its traverse of the clouds; when the average particle size exceeds the wavelength, it is a wavelength-independent quantity. When the average particle size is smaller than the wavelength, τ_1 generally decreases with increasing wavelength. Equations similar to eqs. (3)-(7) have been obtained previously by Neiburger (1949), who used, however, a factor of 1/2 for the average value of μ in eqs. (2).

A comparison of eqs. (3)-(5) with exact solutions of the transfer equation in a variety of limiting cases reveals that our analytic solutions yield relative values accurate to a few percent, and absolute values accurate to 5 to 10%. Furthermore the comparison also provides us with correction factors which reduce still further the errors in the absolute values.

Because of the difficulty in obtaining approximate angular averages of parameters such as β directly from the Schuster-Schwarzschild approximation, we have compared our approximate solutions with known exact solutions in certain limiting cases. A comparison of eq. (3) with an exact solution for the limiting case $\tilde{\omega}_0 = 1$ and $\exp(\tau_1) >> 1$ (Piotrowski, 1956) suggests a relation between β and the phase function of the form

$$\beta = \frac{1}{2}(1 - \tilde{\omega}_1/3)\ , \tag{8}$$

where $\tilde{\omega}_1$ is the coefficient of the Legendre polynomial of first order in the Legendre polynomial expansion of the phase function. The quantities $\mathcal{R}$, $\mathcal{T}$ and $\mathcal{A}$, as given by eqs. (3)-(5), refer to ratios of fluxes, and, as such, contain no information on the angular variation of reflected or transmitted specific intensities. $\mathcal{R}$, for example, corresponds to the Russell-Bond spherical albedo. Fortunately, however, Russell's phase law implies that the reflectivity of a planet at phase angle 50° is a fixed constant times the Russell-Bond albedo; the constant is very closely independent of the phase law for the albedo (see, e. g., de Vaucouleurs, 1964). Thus the ratio of the reflectivities for two wavelengths at phase angles near 50° is equal to the ratio of the Russell-Bond albedos for these wavelengths. This circumstance allows us to apply eq. (3) to relative albedo measurements made near phase angle 50°, or, alternatively, to obtain the Russell-Bond albedo at a desired wavelength, λ_1, from the Russell-Bond albedo at another wavelength, λ_2, and a measurement of the ratio of the albedos at λ_1 and λ_2 measured near phase angle 50°.

If the real and imaginary parts of the index of refraction are known for a given material, $\tilde{\omega}_0$ and $\tilde{\omega}_1$ can be obtained from Mie scattering calculations. Dr. William Irvine has kindly supplied us with exact values of $\tilde{\omega}_0$ and $\tilde{\omega}_1$, obtained with an IBM 7094 for spherical ice crystals in the 0.2 μ to 150 μ wavelength interval. The coefficients of the zeroth and first order Legendre polynomials are functions of both particle radius, a, and wavelength, λ. When $a >> \lambda$, we find that the exact Mie theory solution for this single scattering albedo is represented to sufficient accuracy by

$$\tilde{\omega}_0 = \frac{1}{2} + \frac{1}{2} \exp(-2\, k_\lambda\, a) \quad . \tag{9}$$

where k_λ is the volume absorption coefficient of the particle. This equation has physical significance. The first term represents the diffraction part of the scattering, and the exponential factor represents the fraction of radiation which is absorbed while traversing the particle. The geometry of the particle enters only as the coefficient of $k_\lambda a$ in the exponential, and it is clear that substantially similar results will apply for non-spherical particles as well.

Observations of Venus by Moroz (1964) and by Bottema et al. (1965) strongly suggest that the Cytherean clouds are composed of ice crystals, a suggestion made earlier (Sagan, 1961) on other grounds. Excluding for the moment the wavelength interval around 2.0μ where the correction for Cytherean CO_2 is rather uncertain, several features have been observed which are diagnostic for ice: a stepwise decrease of albedo from 1.2μ to 1.8μ to 2.3μ, a very sharp decline from 2.3μ to about 3.2μ; and relative maxima at 1.8μ and 2.3μ. At all these wavelengths gaseous absorption by CO_2 and H_2O in or above the Cytherean clouds can be neglected; these reflectivity measurements must pertain to the clouds. The identification of the clouds with ice is further reported by Bottema et al.'s (1965) excellent match of the observations with the reflectivity of an ice cloud produced in the laboratory.

These identifications do depend on the assumption that appropriate allowance for the effects of overlying absorption have been made. We now examine this contention in somewhat more detail. Between 3.0 and 3.4 μ, and between 2.2 and 2.5 μ, there is little CO_2 or water vapor absorption; these segments of the spectra observed by Bottema et al. can be accepted as intrinsic to the clouds, with little reservation. The correction for H_2O vapor near 1.8 μ can be checked against the work of Moroz (1964), who observed between 1.7 and 1.8 μ and also near 2.3 μ where there is little gaseous absorption. Moroz' ratio of 1.8 μ to 2.3 μ albedos agrees with the determination of Bottema et al. This check on the water vapor correction performed by Bottema et al. near 1.8 μ lends support for the similar correction they performed between 2.5 and 2.65 μ.

The primary remaining ambiguity lies in the region around 2.0 μ, where absorption by Cytherean CO_2 is expected. Kuiper's (1962) ground-based near-infrared spectra, performed with a resolution much superior to that of Bottema et al., exhibit prominent carbon dioxide bands at 1.6 μ. If they originate at about the same atmospheric level as the 1.6 μ bands, the 2.0 μ CO_2 bands should appear even stronger in the Venus spectrum. Along with the neighboring hot and isotopic bands, it is possible that they account for the minimum observed near 2.0 μ by both Kuiper and Bottema et al. On the other hand it is difficult to exclude the possibility that the observed 2 μ minimum is partially due to carbon dioxide absorption, and partially due to a lower intrinsic reflectivity of the clouds. Such a lower reflectivity implies that the 2 μ CO_2 absorption takes place at higher altitudes than would otherwise be the case.

However, even if we exclude the region around 2.0 μ, the fit of the laboratory ice cloud to the Cytherean spectrum is very impressive. Both clouds are produced by atmospheric saturation in the presence of condensation nuclei; the detailed correspondence in the wavelengths of dips and rises, and in the overall shape of these spectra denotes detailed agreement, not only in the indices of refraction, but also in the particle size distributions of the Venus and the laboratory particles. The influence of size and composition

on the reflection spectrum will be discussed below, where we show that several independent methods for determining the mean particle radius from the observations yield very similar results, provided the clouds are assumed to be composed of ice. In summary, there appears to be good evidence that the clouds of Venus are composed of ice.

The interaction optical depth of the clouds, τ_1, can be found from the Venus albedo in the 4000 to 13,000 A interval. In this wavelength range, the albedo is found to have a high, nearly constant value (Sinton, 1963; Yessipov and Moroz, 1963; Moroz, 1964). These observations are remarkable, because in the same wavelength interval, the absorption coefficient of ice is changing by many orders of magnitude. The results can only be understood if $\tilde{\omega}_0$ is sufficiently close to unity that the cloud albedo is controlled only by τ_1; e. g., a change in $\tilde{\omega}_0$ from 0.9999999 to 0.99999 would then have little influence on the observed albedo, while a change from 0.99 to 0.50 would have a major influence [see eqs. (3), (6), and (7), for the case of slowly-varying β]. The deduction that $1 - \tilde{\omega}_0 \ll 1$ at these wavelengths is supported by the values of $\tilde{\omega}_0$ deduced either from Mie theory or from eq. (9) for particles in the expected size range. We obtain from eqs. (3), (6), and (7) and the Mie theory values of β a value of τ_1 for Venus between 18 and 43; the uncertainty in τ_1 is chiefly a consequence of the observational error in the visible and near infrared cloud albedo. These values of τ_1 are much larger than the values which would have been obtained for isotropic scattering ($\beta = 1/2$) from the same albedo observations. The difference illustrates the highly forward scattering behavior of ice crystals at these wavelengths.

At longer wavelengths, the single scattering albedo decreases significantly below unity and becomes the dominant factor in eq. (3). There is then little dependence of overall reflectivity on τ_1, since the derived values of $\mathcal{R}$ are close to the values for a semi-infinite cloud layer. Through eq. (9), we can then extract from the observations several independent estimates of the mean particle radius, $\bar{a}$.

We obtain $\bar{a}$ from (1) the absolute value of the albedo at 2.5 μ; (2) the ratio of the albedos at 1.2 μ and 1.75 μ; and (3) the relative albedo variation between 1.75 μ and 3.4 μ. The observational value of the Russell-Bond albedo at 2.5 μ was obtained from the Russell-Bond albedo at 0.55 μ (Sinton, 1963), the albedo ratio near 50° phase angle of observations at 0.55 μ and 2.2 μ (Moroz, 1964), and the albedo ratio near 50° phase angle of observations at 2.2 μ and 2.5 μ (Bottema, et al., 1965). The observed albedo ratio at 1.2 and 1.75 μ was obtained from Moroz' (1964) data. Comparisons of theory and observation are provided for the first two methods in Table 1, and, for the third, in Figures 1 and 2. In the figures, the region near 2.3 μ carries little weight, because k_λ is relatively poorly known in this low-absorptivity region. We see from the Table and the Figures that all three methods yield a mean particle radius for ice crystals,

$$7.5\,\mu \leq \bar{a} \leq 10\,\mu\,. \tag{10}$$

The mutual agreement of the results of these independent methods supports the identification of ice as the principal constituent of the clouds of Venus. Even liquid water differs significantly from ice in its values of k_λ. Bound water of crystallization should exhibit even larger deviations in absorption coefficient; and while dust containing water of crystallization will exhibit some similarities in reflectivity with ice, a detailed agreement is not to be expected.

Our estimates of $\bar{a}$ are compatible with the values of $\bar{a} \simeq 1\,\mu$ found from polarization measurements (Dollfus, 1961). We believe the difference in values of $\bar{a}$ can be attributed to two causes. First, the weighting function in the averaging over the particle size distribution to derive $\bar{a}$ is different for polarization than for reflectivity, and will lead to more of the small end of the distribution function sampled during polarization measurements. Secondly, since multiple scattering depolarizes, the polarization measurements refer chiefly to photons scattered once, or at most a small number of times. If there is any tendency for particle size sedimentation in the

TABLE 1

COMPARISON OF THEORETICAL AND OBSERVED VALUES OF THE ALBEDO OF VENUS

		A(2.5 μ)		A(1.75 μ)/A(1.2 μ)	
		$\tau_1 = 18$	$\tau_1 = 43$	Minimum τ_1	Maximum τ_1
OBSERVED VALUE		0.34 ± 0.05		0.81 ± 0.04	
THEORETICAL VALUES					
MEAN PARTICLE RADIUS	1 μ	0.41	0.56	0.980	0.958
	2	0.61	0.64	0.967	0.933
	4	0.51	0.52	0.944	0.894
	6	0.44	0.44	0.903	0.832
	7.5	0.39	0.40	0.862	0.780
	10	0.32	0.32	0.816	0.728
	12.5	0.27	0.27	0.773	0.684
	15	0.24	0.24	0.737	0.650
	20	0.19	0.19	0.666	0.589

Minimum τ_1 and maximum τ_1 are the minimum and maximum values for τ_1 implied by the 0.4 μ to 1.3 μ albedo for a given particle size. For $\bar{a} = 7.5$ μ, the values are $\tau_1 = 18$ and 43. For other particle sizes, the values of τ_1 are slightly different.

Cytherean clouds, the polarization measurements will refer to higher levels in the clouds, where mean particle sizes are smaller, than the levels probed by reflectivity measurements.

The location of relative maxima and minima in the spectra of Bottema et al. (1965) also permit a crude estimate of temperature to be derived. The balloon observations unambiguously show relative maxima at wavelengths of approximately 1.82 μ and 2.28 μ. These peaks correspond well to minima in k_λ and, therefore, maxima in $\tilde{\omega}_0$ for ice crystals, but are distinctly longward of the corresponding peaks for liquid water (1.67 μ and 2.22 μ) at room temperature. But temperature declines will shift both minima and maxima to longer wavelengths. Thus we may conclude that the observed albedo is a consequence of multiple scattering in regions of the Cytherean clouds which were below 0° C, in agreement with the expected thermometric temperatures of the clouds (Pollack and Sagan, 1965).

The foregoing estimates of composition τ_1, and $\bar{a}$ permit us to determine the optical properties of the clouds at all wavelengths. We find that between 20% and 50% of the sunlight absorbed by the planet reaches the surface; the remainder of the absorbed sunlight is accounted for in approximately equal parts by the clouds and by the underlying atmosphere. Due to absorption by water vapor and carbon dioxide, and the high surface pressures and temperatures, the Venus atmosphere is fairly opaque beyond 1 μ. The clouds have an enormous opacity beyond 2.65 μ. Because they are poorly absorbing and anisotropically scattering in the visible and photographic infrared, but strongly absorbing and almost isotropically scattering at longer wavelengths, the clouds provide the additional differential opacity required to establish an effective greenhouse effect and maintain surface temperatures ~700° K (cf. Sagan, 1960; Ohring and Mariano, 1964). The clouds serve chiefly by plugging holes in the principal atmospheric infrared windows. The value of the surface temperature is determined by the height of the ice clouds in the convective Cytherean atmosphere; this height depends, in turn, on the total atmospheric water vapor content. Our calculations show that the cloud bottoms have a quantity of supercooled water droplets (~ 0.1 gm cm^{-2}) too

small to influence significantly the reflection spectrum, but adequate to account for the general features of the millimeter wavelength spectrum of Venus. These and related consequences of the water clouds of Venus are discussed in greater detail elsewhere (Sagan and Pollack, 1966).

Acknowledgments

We are very grateful to Dr. William Irvine for providing us with Mie theory solutions for ice and water under a variety of assumed condition; to Dr. John Strong for a discussion of his laboratory observations; and to Mrs. Elinore Green for assistance with the calculations. The final phases of this investigation were supported by NASA grant NGR 09-015-023.

REFERENCES

Bottema, M., W. Plummer, J. Strong, and R. Zander, The composition of the Venus clouds and implications for model atmospheres, J. Geophys. Res., 70, 4401-4402, 1965.

Chandrasekhar, S., "Radiative Transfer", Oxford University Press, London, 1950.

Dollfus, A., Polarization studies of planets, in, "Planets and Satellites," edited by G. P. Kuiper and B. M. Middlehurst, pp. 343-399, U. Chicago Press, Chicago, 1961.

Kuiper, G. P., Infrared spectra of stars and planets, I: photometry of the infrared spectrum of Venus, 1-2.5 microns, Comm. Lunar and Planetary Laboratory, 1, 83-118, 1962.

Moroz, V. T., Infrared spectrum of Venus (1-2.5μ), Soviet Astron. J., English Transla., 7, 109-115, 1964.

Neiburger, M., Reflection, absorption and transmission of insolation by stratus clouds, J. Meteorology, 6, 98-104, 1949.

Ohring, G., and J. Mariano, The effects of cloudiness on a greenhouse model of the Venus atmosphere, J. Geophys. Res., 69, 165-175, 1964.

Pollack, J. B., and C. Sagan, The infrared limb-darkening of Venus, J. Geophys. Res., 70, 4403-4426, 1965.

Piotrowski, S., Asymptotic case of the diffusion of light through an optically thick scattering layer, Acta Astronomica, 6, 61-73, 1956.

Sagan, C., The radiation balance of Venus, Jet Propulsion Lab. Tech. Rep. 32-34, 1960.

Sagan, C., and J. B. Pollack, On the nature of the clouds and the origin of the surface temperature of Venus, Icarus, to be published.

Sinton, W. M., Infrared observations of Venus, in "Physics of Planets," Proc. XI Intl. Astrophys. Symp., Liege, Belgium, pp. 300-310, 1963.

de Vaucouleurs, G., Geometric and photometric parameters of the terrestrial planets, Icarus, 3, 187-235, 1964.

Yessipov, V. F., and V. I. Moroz, "An attempt at spectrophotometry of Venus and Mars in the interval 7000-10,000 Å, "Astron. Tsirkulyar No. 262 (in Russian) 1963.

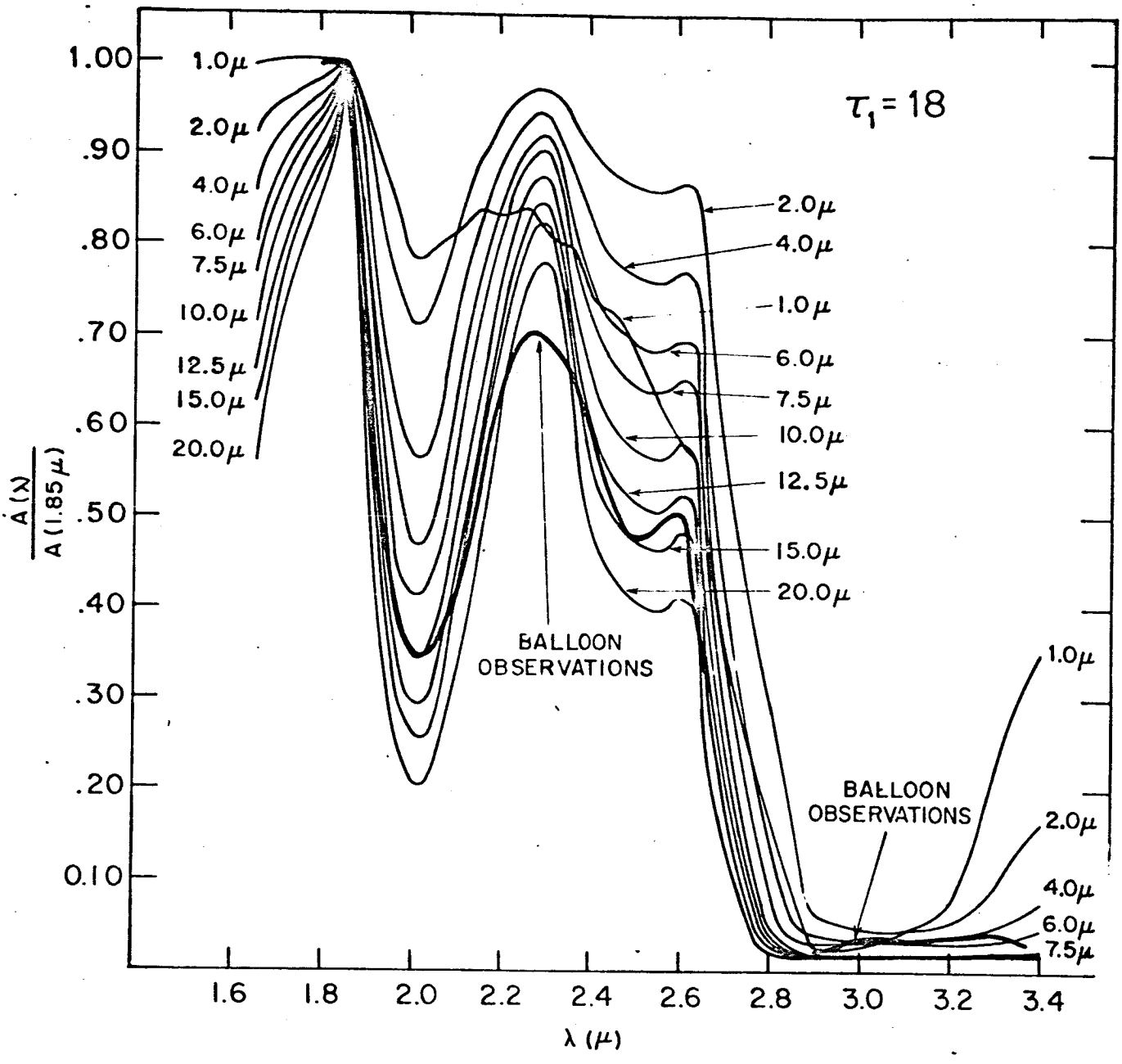

Figure 1. Comparison of Theoretical and Observed Normalized Infrared Reflectivities of Venus for Particle Radii 1-20μ and $\tau_1 = 18$.

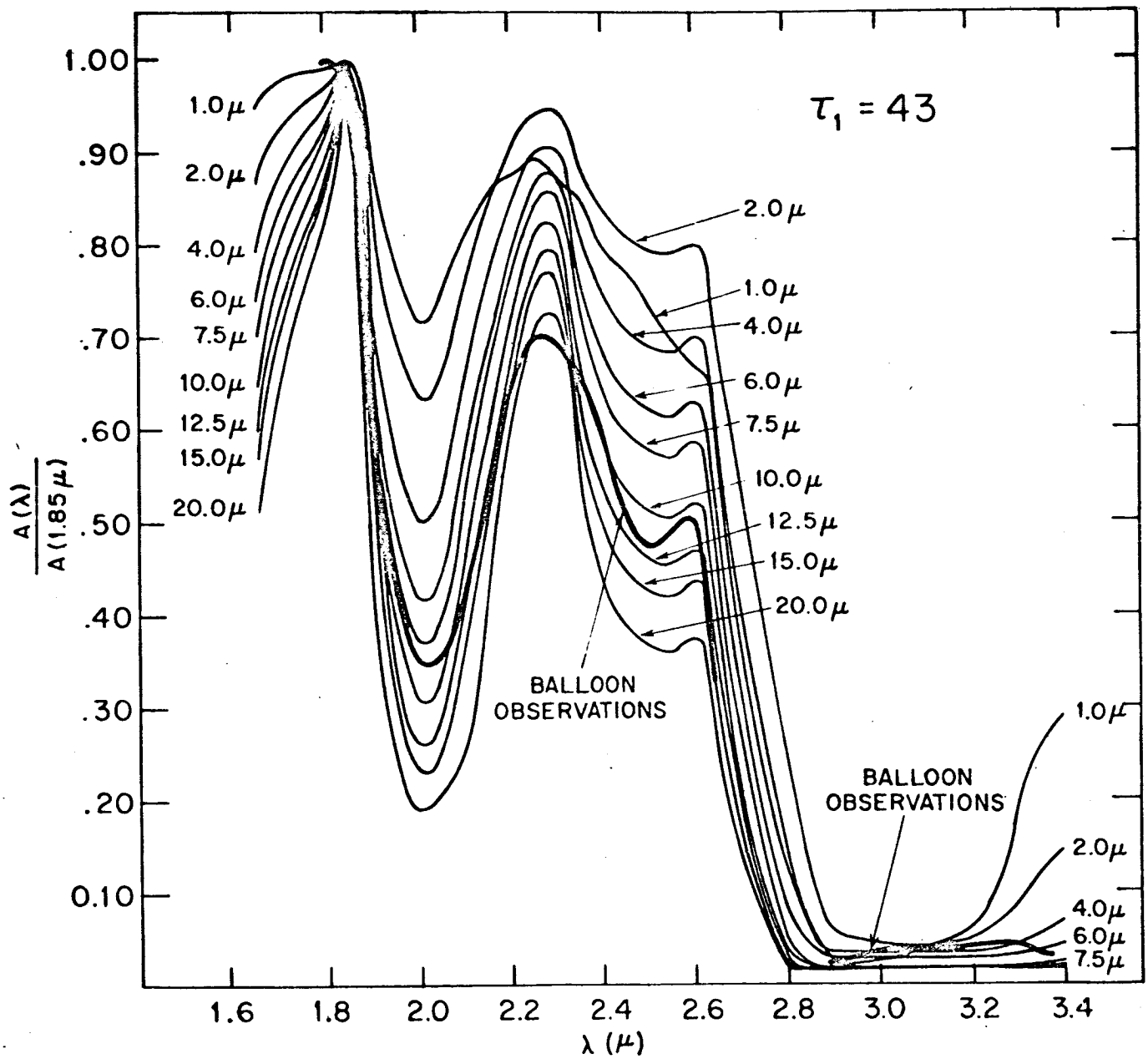

Figure 2. Comparison of Theoretical and Observed Normalized Infrared Reflectivities of Venus for Particle Radii 1-20μ and $\tau_1 = 43$.

THERMODYNAMIC EQUILIBRIA IN PLANETARY ATMOSPHERES

Ellis R. Lippincott

Department of Chemistry
University of Maryland, College Park

Richard V. Eck

National Biomedical Research Foundation
Silver Spring, Maryland

Margaret O. Dayhoff

National Biomedical Research Foundation
Silver Spring, Maryland

Carl Sagan

Harvard University

and

Smithsonian Astrophysical Observatory
Cambridge, Massachusetts

Revised _____

Smithsonian Institution
Astrophysical Observatory
Cambridge, Massachusetts 02138

THERMODYNAMIC EQUILIBRIA IN PLANETARY ATMOSPHERES

Ellis R. Lippincott, Richard V. Eck,
Margaret O. Dayhoff, and Carl Sagan

Abstract

The thermodynamic equilibrium composition of all possible combinations of the elements C, H, O, and N at reasonable average pressures and temperatures have been calculated for the atmospheres of Earth, Venus, Mars, and Jupiter. All regions of the composition diagram consistent with the observed molecular abundances are located and discussed.

The constituents of the terrestrial atmosphere are in approximate thermodynamic equilibrium in spite of the continual addition of trace compounds by biological activity, lightning, radiation, and vulcanism. Under some circumstances, the presence of atmospheric organic molecules far in excess of their thermodynamic equilibrium proportions can be an indication of indigenous biological activity.

The atmosphere of Venus seems likely to be in thermodynamic equilibrium. It then follows that the measured upper limits on the abundances of CH_4, NH_3, and CO are all inconsistent with the possibility of elemental carbon or hydrocarbons in contact with the atmosphere, either on the surface or as clouds. If the Cytherean atmosphere evolved from an original gas mixture much more reducing than the present, two processes must have occurred: the loss of hydrogen to space and the loss of O_2, most probably by efficient reaction with a considerable layer of reduced surface materials. In addition, Venus must have begun its evolutionary history with a [C/O] abundance ratio ≤ 0.5, a value consistent with several cosmic abundance estimates.

The evidence for Mars is not inconsistent with thermodynamic equilibrium. The computations do not indicate whether small quantities of free O_2 exist. The equilibrium abundances of all oxides of nitrogen are extremely low even if computed with a considerable excess of O_2.

For Mars and Venus there are no molecular species with a large predicted equilibrium abundance and spectroscopically accessible absorption features which have not already been identified.

Under equilibrium conditions at low temperatures Jupiter also cannot contain significant amounts of any molecule not yet observed. However, at high temperatures such as would be produced by lightning discharges or in the Jovian thermosphere, simple hydrocarbons and cyanides, polycyclic aromatics, and a variety of nitrogen compounds would be expected. Some of these compounds are brightly colored, and it seems possible that such organic compounds contribute to the observed variable coloration of Jupiter.

1. Introduction

The gross chemical composition of planetary atmospheres can be approximated to some degree as the thermodynamic equilibrium distribution of the constituent atoms. In the upper reaches of planetary atmospheres, where the optical depth at ultraviolet frequencies is small, relative molecular abundance may be dominated by photodissociation and recombination. In the lower portions of the atmospheres, which are shielded from photodissociating ultraviolet radiation, a closer approximation to thermodynamic equilibrium can be expected. Especially where surface temperatures are high or when catalysts such as water are present, there will be a strong tendency for the degradation of molecules to the lowest energy state. Even in the presence of special mechanisms which favor the production of specific compounds -- mechanisms such as ultraviolet radiation or lightning -- the thermodynamic equilibrium distribution of reaction products should be a useful first-order approximation. Since the equilibrium state is independent of particular reaction mechanisms and reaction rates, and since the computations of equilibrium states are quite straightforward, studies of thermodynamic equilibrium chemistry would appear prerequisite to considerations of nonequilibrium processes.

One of the earliest examples of a fruitful argument from thermodynamic equilibrium in planetary atmospheres was provided by Wildt (1937), who pointed out that the absence of detectable amounts of higher hydrocarbons, both saturated and unsaturated, in the atmospheres of

the Jovian planets was an argument for the presence of a great excess of molecular hydrogen, a gas which had not been detected at that time. Further indirect evidence for the presence of low-mass constituents in the Jovian atmosphere was provided by observations of the occultation of σ Arietus, by Baum and Code (1953); but not until fairly recently were the quadrupole lines of H_2 observed directly in the photographic infrared (Kiess, Corliss, and Kiess 1960). Urey (1959) has argued from the large abundance of carbon dioxide on Venus that substantial quantities of CH_4, NH_3, H_2, N_2O, and other oxides of nitrogen would not be expected on that planet. A very low upper limit on the allowed abundance of oxides of nitrogen in the Martian atmosphere was set by Sagan, Hanst, and Young (1965) in a discussion of combined photochemical and thermodynamic equilibria. Wildt (1937) and Urey (1952), while performing thermodynamic equilibrium calculations in a planetary atmospheres context, stressed the possibility of significant departures from thermodynamic equilibrium.

Some more recent studies have suggested that thermodynamic equilibrium calculations may, under certain circumstances, be a useful approximation to reality. Thermodynamic equilibrium calculations by Dayhoff, Lippincott, and Eck (1964) for the relative abundances of a large number of compounds of biological interest have been performed under a wide variety of assumed conditions of temperature, pressure, and elemental composition. These machine computations have revealed a possible mechanism for the abiological formation of polycyclic aromatic hydrocarbons (asphaltic tars) and have shown the existence of an oxidation threshold where free oxygen appears and at which all but the simplest organic compounds disappear. Studier, Hayatsu, and Anders (1965) have recently called attention to a remarkable agreement between the distribution of organic compounds observed in the carbonaceous chondrites, and that which we predicted

from thermodynamic equilibrium calculations in the range of elemental abundances where asphaltic tars are expected. This success has encouraged us to extend thermodynamic equilibrium calculations to planetary atmospheres.

2. Methods of Calculation

Our computational procedures have been described previously (Dayhoff, Lippincott, and Eck 1964) following a well-known method (White, Johnson, and Dantzig 1958) which minimizes the free energy of the system, simultaneously satisfying the equilibrium constants of all possible reactions. The calculations were performed on an IBM 7094 computer.

At thermodynamic equilibrium, the distribution of molecular species is independent of the specific reaction pathways by which equilibrium is attained. The molecular balance depends upon the relative elemental abundances, pressure, temperature, and the standard free energies of formation of the compounds. All compounds present in significant concentrations must be included in order to arrive at the correct molecular distribution. Fortunately, there are only a small number of these major compounds; they are simple in structure and well known to chemists. For a real system to approach equilibrium, there need be only one reversible reaction pathway which leads from the major constituents to the other compounds.

In our computations on planetary atmospheres, we explored the entire range of possible relative atomic compositions using a large number of molecular species in order to locate any specific ranges of atomic abundances which would be simultaneously compatible with all the existing estimates of molecular abundances or their upper limits.

The results are presented in ternary diagrams which cover all possible proportions of the elements C, H, and O. Compounds of nitrogen can also be represented as a projection on this diagram. The astronomical observation of a specific relative abundance for a given molecular species will, in general, define a line on the ternary diagram. An upper or lower concentration limit will exclude a certain area. The application of several such constraints may operate in a mutually inconsistent manner, so that no point on the diagram simultaneously satisfies all observations. In such a case, we would conclude that thermodynamic equilibrium is not attained in this atmosphere. On the other hand, if the application of several such constraints can be performed in a consistent manner, yielding a region of the ternary diagram simultaneously compatible with all constraints, we might tentatively conclude that thermodynamic equilibrium is a useful first approximation to the atmosphere in question. Each point in the allowed region of the diagram would then correspond to a possible elemental composition in the planetary atmosphere. The calculations would place some upper and lower limits on the allowable relative abundances of other possible constituents of the atmosphere.

3. Observational Limitations

The initial conditions for these computations are based upon the results of astronomical spectroscopy. It is not a trivial matter to derive relative abundances from such observations. The conversion of equivalent widths to absolute abundances requires careful laboratory calibrations. Intercomparisons of abundances derived for the same molecule at different wavelengths must allow for the possibility that the effective reflecting atmospheric level is a function of wavelength. Existing observational discrepancies on, for example, the abundance of water vapor in the atmosphere of Venus (see, e. g., the discussion

by Sagan and Kellogg 1963) underscore the uncertainties of such reductions. Intercomparisons of the relative abundances of different molecular species is even more uncertain. Determinations of absolute abundances is complicated by the possibility of multiple scattering (see Chamberlain 1962, 1965). Observations of very weak lines of a given molecular species may refer to substantial depths in the planetary atmosphere, where ultraviolet photodissociation is not a dominant process. Observations of strong lines may refer to high altitudes alone, where the relative distribution of molecular species may be far from that predicted by thermodynamic equilibrium. However, the species must be derivable from some compounds present extensively in the atmosphere.

Bearing these cautions in mind, we now proceed to a discussion of thermodynamic equilibrium in the atmospheres of the planets Earth, Venus, Mars, and Jupiter. In general, the conclusions we will draw will not be sensitively dependent on the exact values of the adopted mixing ratios of minor constituents; and variations in these mixing ratios even by several orders of magnitude will leave most of the results unchanged. Thus, despite the uncertainties in the observational material, it will nevertheless be possible to draw conclusions of some significance.

4. The Earth

As a test of our computation procedures, we first consider thermodynamic equilibrium in the terrestrial atmosphere. In addition to its major components, the atmosphere of the Earth contains a variety of compounds of diverse origins: methane and smaller amounts of other hydrocarbons from natural gas, petroleum, and asphalt; sulfur dioxide, hydrogen sulfide, carbon monoxide, and nitrogen oxides from vulcanism;

terpenes and other volatile organics from vegetation; methane, N_2O, and hydrogen sulfide from the metabolic processes of microorganisms; ozone and nitrogen oxides from lightning and solar radiation, etc. Table 1 shows the amounts of some of these compounds which have been detected in the open air.

We have calculated the balance of compounds for every combination of C, H, O, and N at 1 atm and 280°K. The only equilibrium consistent with the observed major constituents in Table 1 is shown in Table 2. Such a point where major constituents in the terrestrial atmosphere are completely compatible with thermodynamic equilibrium need not necessarily exist. For example, large quantities of CO, natural gas, or H_2S might be admixed. All of these would decompose at thermodynamic equilibrium in the presence of excess oxygen. Any carbon in the atmosphere would occur as CO_2, and any sulfur as SO_3. Since there is no reason to think that less oxidized materials are presently accumulating in the atmosphere, they must be in approximate dynamic equilibrium, being removed or destroyed as fast as they are being added. That is, even at the prevailing low temperatures there is a definite tendency for the Earth's atmosphere to approach thermodynamic equilibrium. Such reactions are no doubt catalyzed by solar radiation and by dust particles and droplets suspended in the air. This constitutes a specific example of our general contention that, even in the presence of special mechanisms which favor the production of certain specific compounds, the overall tendency will be for a planetary atmosphere to approach thermodynamic equilibrium. If the major components of the atmosphere were methane, hydrogen, water, and nitrogen (or ammonia) instead of the present composition, the products of the radiation-coupled reactions would be different, but the overall trend to thermodynamic equilibrium would still be present. It is not obvious at what relative rates unstable

prebiological compounds such as amino acids would be produced by nonequilibrium processes and degraded by the environment and by their interaction with each other.

The observation of complex, very energetic compounds such as terpenes in the contemporary atmosphere of the Earth would lead an extraterrestrial observer to suspect the existence of life here. The lack of any obvious simple mechanism to form terpenes, either by thermodynamic equilibrium at some plausible combination of elemental composition, temperature, and pressure, or by photochemical reactions or other physical processes, would indicate the presence of biological activity on the Earth -- even in the absence of any other signs of life. Simpler highly reduced substances also exist far in excess of their thermodynamic equilibrium proportions in the oxidizing terrestrial atmosphere -- e.g., CH_4 (compare Tables 1 and 2). Such materials would therefore also be a possible test for indigenous biology; but since other plausible origins could be imagined for them -- e.g., the decomposition of prebiologically synthesized polycyclic aromatics -- the presence of such molecules would be inconclusive for biology. In fact, methane has such a high abundance in the terrestrial atmosphere only because of the metabolic activities of microorganisms (see, e.g., Hutchinson 1954).

5. Venus

The observational constraints on the atmospheric composition of Venus are given in Table 3, constructed from the references there given. Some comments should be made on the values adopted for $[CO_2]^*$, $[H_2O]$, and $[CO]$. The 5% volume mixing ratio of carbon dioxide adopted in our analysis is a fairly conventional one, derived from Spinrad's (1962a) observations, and dependent upon the assumption that the near infrared CO_2 bands are formed by single scattering. Chamberlain (1965) has recently shown that the introduction of multiple scattering might reduce the CO_2 mixing ratio by as much as an order of magnitude. The precise reduction factor is at the present time unknown. However, similar correction factors for multiple scattering will be applicable to all other abundances and abundance upper limits of Table 3, and relative abundances of all minor constituents should be approximately those of Table 3, whether single or multiple scattering is assumed. The relative abundance of the major atmospheric constituents -- probably N_2, with some admixture of noble gases -- would then vary from 95% to larger values. Such variations have no significant effects on our conclusions.

Reported observations of water vapor in the spectrum of Venus have been made by Dollfus (1964) and by Bottema, Plummer, and Strong (1964). The derived values of the water vapor mixing ratio depend on the scattering mechanism and the total atmospheric pressure at the effective level of band formation. The range of derived mixing ratio values shown in Table 3 is consistent (Sagan and Kellogg 1963, Chamberlain 1965) with a previous upper abundance limit on water vapor established by Spinrad (1962b). However, the water vapor which is observed by infrared spectroscopy may be primarily in the region of the clouds. Since there is now fairly convincing evidence that the clouds

*In the following discussion square brackets denote volume mixing ratios.

are condensed water (Bottema, Plummer, Strong, and Zander 1964, Sagan and Pollack 1966a), it is in general invalid to assume that the water vapor mixing ratio in the vicinity of the clouds applies to the lower Cytherean atmosphere. The amount of condensed water in the clouds required to explain the near infrared reflection spectrum of Bottema, Plummer, Strong, and Zander (1964), and also to explain the millimeter attenuation of the surface thermal microwave emission, is 1 gm cm^{-2} or less; convective atmospheres which can maintain such clouds at the observed pressures and temperatures must have volume mixing ratios of water vapor in their lower reaches of a few times 10^{-4} (Sagan and Pollack 1966b). The water vapor mixing ratio may therefore range from a few times 10^{-6} in the vicinity of the clouds and above, to a few times 10^{-4} near the Cytherean surface.

The quantities of carbon monoxide in the spectrum of Venus observed by Moroz (1965), if related to a 1 atm pressure level near the cloudtops, give a volume mixing ratio $\sim 10^{-6}$. However, CO is a principal carbon dioxide photodissociation product, and amounts of carbon monoxide almost comparable to those reported by Moroz may arise from photodissociation (Moroz 1965, Shimizu 1963). If the observed carbon monoxide abundance is significantly in excess of that expected from photochemical equilibrium, then a CO mixing ratio of 10^{-6} may be extended down to the lower Cytherean atmosphere. If, on the other hand, the observed carbon monoxide is due principally to photochemical processes, then the carbon monoxide abundance in the lower Cytherean atmosphere will be substantially less.

We adopt a Venus surface temperature of 700°K, and a surface pressure of 50 atm (Sagan 1962, Pollack and Sagan 1965). Moderately large departures from these values will not alter our conclusions significantly. In particular, the calculations performed at such pressures

and temperatures should, because of the relative pressure and temperature insensitivity of the reaction thresholds and because of atmospheric convection, be applicable to a major fraction of the total mass of the Cytherean atmosphere.

A ternary diagram showing all possible combinations of the elements C, H, and O is presented in Figure 1. The corners of the triangle represent pure carbon, pure hydrogen, and pure oxygen. The positions of pure carbon dioxide and pure water are also indicated. The line connecting the CO_2 and H_2O points is an oxidation threshold, which divides the diagram into an upper, reducing, portion in which sizable numbers of different species of organic molecules may be expected at thermodynamic equilibrium, and a lower, oxidizing, portion, in which such molecules are unstable, and in which free oxygen exists. Also indicated in Figure 1 is the asphaltic tar threshold. Above this line, polycyclic aromatic hydrocarbons occur at thermodynamic equilibrium (in the absence of a mechanism to form graphite); below it, they are excluded. Since graphite is not observed in heat-catalyzed reactions involving temperatures of 700°K (Studier, Hayatsu, and Anders 1966) and in quenched plasmas (Eck, Lippincott, Dayhoff, and Pratt 1966), the computations have been extended past the line of graphite precipitation.

The ammonia upper abundance limit of 4×10^{-7} restricts the atmosphere at thermodynamic equilibrium to the region below the line marked NH_3 in Figure 1. This line lies in the reducing region of the diagram, slightly above the oxidation threshold, and curves away from the carbon dioxide point, as illustrated. This one spectroscopic upper limit therefore excludes most of the reducing portion of the ternary diagram. The concentration of ammonia varies so rapidly in the region of the illustrated line that the width of this line represents several orders of magnitude in concentration -- an example of the insensitivity of these calculations to exact relative abundances.

We next consider the upper abundance limit on methane. This concentration yields a curve which closely follows the C-O edge until the CO_2 point is reached, whereupon it swings away and follows the oxidation threshold. The CH_4 curve is even more constraining than the NH_3 curve, and excludes almost the entire reducing portion of the diagram.

We now consider the constraints imposed by the water vapor mixing ratio. Figure 1 shows a line for $[H_2O] = 10^{-5}$, which, in the oxidizing region of the diagram, lies very close to the C-O edge. The curves for mixing ratios an order of magnitude larger would lie very close to the curve shown. Thus, the searches for methane, ammonia, and water have restricted the equilibrium chemistry of the Cytherean atmosphere to a very narrow region of the ternary diagram, hugging the C-O edge throughout the oxidizing region, and extending very slightly into the reducing region.

In Figure 2, where the Venus ternary diagram has been magnified 100 times, the line corresponding to a carbon monoxide volume mixing ratio of $[CO] = 10^{-6}$ is indicated. Since part of the observed carbon monoxide may be due to CO_2 photodissociation, the fraction of carbon monoxide relevant for thermodynamic equilibrium calculations will be somewhat less than 10^{-6}. The observations therefore further restrict the ternary diagram to the area below the line $[CO] = 10^{-6}$. We see that this line closely parallels the oxidation threshold. As with the NH_3 and CH_4 lines, the width of the $[CO] = 10^{-6}$ line actually corresponds to many orders of magnitude in the mixing ratio. The lower side of this line corresponds to the oxygen upper abundance limit, 8×10^{-5}. If observations can establish any detectable amount ($> 10^{-16}$) of CO in the lower atmosphere, the amount of O_2 must be extremely small. Conversely, if $[O_2] \geq 8 \times 10^{-5}$, the $[CO] \leq 4 \times 10^{-17}$. At any rate the upper limits on Cytherean [CO] and $[O_2]$ restrict the thermodynamic equilibrium composition to the thickness of the thick slant line in Figures 1 and 2.

In Figure 2 is displayed a line above which a solid phase of graphite might form. The composition of the atmosphere is clearly incompatible with solid carbon in equilibrium in the atmosphere or on the surface. Similarly, any equilibrium accumulation of polycyclic aromatics, or any other hydrocarbons, is forbidden, a conclusion reached for a much smaller array of compounds by Mueller (1964). The asphalt threshold seen in Figure 1 lies well into the region excluded by the unsuccessful searches for CH_4 and NH_3. This conclusion is separately confirmed by the CO upper abundance limits, and is independent of the quantity of water present. This exclusion of hydrocarbons is relevant to some models of the Venus atmosphere which invoke hydrocarbon clouds (Kaplan, 1963). The absence of polycyclic aromatic hydrocarbons from the surface is consistent both with passive observations of the microwave phase effect and with active radar observations of Venus (Pollack and Sagan, 1965).

Table 4 shows the chemical composition of the atmosphere of Venus, at two extremes of CO and O_2 concentration, predicted from thermodynamic equilibrium. If the measured value of CO depends entirely on photodissociation, then there may be as much as $[O_2] = 8 \times 10^{-5}$. We emphasize again that any error in the relative abundance of nitrogen would cause negligible deviation in the relative abundance of carbon compounds, and indeed, would have very little effect on the calculated ammonia abundance. A smaller amount of nitrogen would only make the ammonia concentration a less severe restriction on the actual composition (cf. Figure 1). The constituents shown at the bottom of the table would be formed if 0.0001% sulfur were added to the atmosphere.

Formaldehyde was once suspected in the atmosphere of Venus (Wildt, 1940) but at thermodynamic equilibrium with the detected amounts of water and the observational upper limit on methane; the concentration of formaldehyde would be negligible. Non-equilibrium reactions in

simulated Cytherean atmospheres are known, however, to produce formaldehyde (Sagan and Miller, 1960).

We now explore some other consequences of the foregoing abundances. Possible atmospheric compositions are limited to a segment of the $[CO] = 10^{-6}$ curve near $[H_2O] = 10^{-4}$, as shown in Figure 2. The composition of Venus is then specified by a segment of one thick line in the ternary diagram, near the CO_2 composition point, and slightly on the reducing side of the oxidation threshold. This conclusion is consistent with all abundance determinations and upper limits. The fact that none of the observations are mutually inconsistent suggests that the atmosphere of Venus is, on the whole, close to that predicted by thermodynamic equilibrium.

It should be emphasized that the finding that the predicted thermodynamic equilibrium is consistent with the available observations is not trivial. Whatever the given molecular species used to define a particular atomic composition of the atmosphere, the computed equilibrium molecular proportions would be the same. Neither can one predict a priori which of the major compounds would be present, given a particular elemental composition. The proportions 1 C: 2 H: 2 O give the empirical formula of formic acid, but this compound would be only a minor component of the equilibrium mixture. The same proportions apply to an equimolar mixture of CO and H_2O. However, a gas composed of these two compounds is not the correct answer, either. The equilibrium result is a mixture of H_2O, CH_4, and CO_2--unless the computation had been for a higher temperature, in which case there would also have been appreciable amounts of CO and H_2.

A disagreement between predicted and observed results can occur in two ways. First, a definite observed species may be unobtainable at equilibrium. If 1 percent of HCN had also been observed on Venus,

we would have found no C: H: O proportions for which this large amount would be predicted. Such an observation would have been inconsistent with the hypothesis of thermodynamic equilibrium on Venus.

Secondly, all systems consistent with the observed concentrations could also contain observable quantities of compounds which were not in fact observed. Such inconsistencies were sought, but not found. We therefore conclude that the results are consistent with general thermodynamic equilibrium on Venus; only a very limited fraction of the atmosphere is being produced by such special processes as discussed for the earth's atmosphere.

In this case some remarks can be made on the original composition and subsequent evolution of the Cytherean atmosphere. From cosmic abundance considerations, it is clear that the atmosphere must originally have had a composition putting it in the extreme right-hand corner of the ternary diagram (cf. Figure 3), if the atmosphere was originally derived from a solar nebula. If it was derived from vulcanism, the composition would have been somewhere in the middle of the reducing region, and the following considerations would apply just as well. The chemical evolution of the atmosphere occurs initially through the escape of atomic hydrogen from the Cytherean exosphere. Escape of significant quantities of carbon or oxygen from Venus during geological time seems quite unlikely (see, e.g., Sagan, 1966). Any differential escape is correspondingly unlikely. The track along which the atmospheric composition of Venus evolves depends then on the initial carbon-to-oxygen abundance ratio. The cosmic [C/O] abundance ratio has been assigned a value of 0.20 by Suess and Urey (1956), while Cameron (1959) has suggested a value of 0.44 and more recently (1963), 0.67. For a ratio of 0.20 or 0.44, the evolution would proceed along the lines ending at α or β (Figure 3), in a region where free oxygen exists. For

an initial [C/O] ratio of 0.67, the evolutionary track ends at γ, in the reducing portion of the diagram. The actual present atmosphere of Venus appears to have a [C/O] ratio that differs from that of CO_2 by an amount 10^{-5} or less. If the initial atmosphere had a C/O ratio anywhere between 0.2 and 0.7, the probability that the present ratio would be as close to CO_2 as it appears to be, through no other process but the loss of hydrogen, would then be about 4×10^{-5}. This seems quite unlikely. However, if oxygen were also depleted from the atmosphere, then over a wide range of initial [C/O] ratios the atmosphere would finally settle at the CO_2 point. Since it seems unlikely that oxygen has escaped from Venus, the depletion of atmospheric oxygen must be attributed to chemical reactions, and the surface material of Venus, initially reducing, must now be partially oxidized to a considerable depth. An independent argument for the presence of extensive oxygen sinks on the surface of Venus has been offered by Sagan (1966), in an attempt to explain the differential abundance of water on Venus and on Earth by differential rates of water photodissociation.

Typical evolutionary tracks would then have resembled those illustrated by the arrows in Figure 3. Due to loss of hydrogen, the atmosphere evolves away from the hydrogen corner of the ternary diagram until it intersects the oxidation threshold. As soon as free oxygen is produced, it combines with surface material and the evolutionary track turns abruptly upward, following the oxidation threshold toward the CO_2 point.

If the initial [C/O] ratio were 0.44, the initial evolutionary track due to the loss of hydrogen would twice intersect the graphite threshold (cf. Figure 3). There would then be an interlude in the evolutionary history of Venus in which graphite might be present. However, the activation energy for the formation of graphite is so great that it would

very likely never precipitate directly. If it did, it would react and disappear as the system lost more hydrogen. Such a track would follow the line marked H-β until it intersected the oxidation threshold, whereupon it would turn and proceed towards the CO_2 point.

If the initial [C/O] ratio were 0.67, the evolutionary track would follow the line marked H-γ in Figure 3. This line intersects the graphite threshold once, and never crosses the oxidation threshold. The atmosphere would then always remain in the reducing portion of the diagram. In order to end at the CO_2 point, some mechanism must exist for the removal of carbon from the atmosphere or the addition of oxygen to it. The asphalt threshold is not intersected, so no formation of polycyclic aromatics would be expected. If the removal of carbon from the atmosphere were possible—for example, by the precipitation of graphite or organic material—the atmosphere would then evolve along the graphite line in Figure 2. The composition would end significantly above the actual composition point, in conflict with the spectroscopic observations. While the outgassing of water, photodissociation, and hydrogen escape could conceivably increase the O_2 abundance over a surface which was <u>not</u> highly reducing, the addition of just enough O_2 to bring the atmosphere to its present intermediate composition is highly implausible.

Thus, it is probable that Venus began its evolutionary history with a [C/O] abundance ratio ≤ 0.5 and that its evolutionary track in the ternary diagram was directed towards the CO_2 point by the simultaneous loss of hydrogen to space and oxygen to the surface.

6. Mars

Because of the low temperature and relative ultraviolet transparency of the Martian atmosphere, the applicability of thermodynamic equilibrium calculations should be more limited than in the case of Venus. The character of the equilibrium state is nevertheless of interest. A surface temperature of 240° K and a surface pressure of 50 mb was assumed for the Martian atmosphere (Kaplan, Munch, and Spinrad, 1964; Hanst and Swan, 1965). Our remarks on the insensitivity of the calculations to the precise values of pressures and temperatures apply again to this case and a surface pressure of 10 mb would not appreciably alter the results. The observational constraints on the atmospheric composition are shown in Table 5. The atmosphere is assumed to be approximately 90% molecular nitrogen and noble gases. The remainder of the atmosphere is expected to be compounds of carbon, oxygen, nitrogen, and hydrogen. The anticipated CO_2 mixing ratio is not known at the present time. Its value is tied closely to the value of the absolute surface pressure (Kaplan, Munch, and Spinrad, 1964; Hanst and Swan, 1965; Chamberlain and Hunten, 1965). The values of Table 5 correspond to the range of suggested values at the time of writing. As in the case of Venus, the absolute value of the CO_2 mixing ratio is not critical in computations of the relative values of the mixing ratios of minor constituents.

The ammonia upper abundance limit excludes the highly reducing portion of the ternary diagram, as shown in Figure 4. The upper limit on the methane mixing ratio imposes a more significant boundary condition, restricting the range of possible atmospheric compositions essentially to the portion below the oxidation threshold, with the exception of a small section of the reducing part of the diagram along the C-O axis. The carbon monoxide upper limit places no new constraint on the diagram; the upper limits on oxygen and ozone

eliminate a region near the oxygen corner of the ternary diagram. The estimate for the abundance of water vapor in the Martian atmosphere places the equilibrium composition along a curve which crosses the oxidation threshold not far from the CO_2 composition point, quite analogous to the situation for Venus. This line quickly enters the region forbidden by the methane abundance upper limits. The composition of the Martian atmosphere is therefore restricted to the solid portion of the water line of Figure 4, encompassing a small region of the oxidizing part of the diagram, and a very small segment, near CO_2, in the reducing region.

It has been suggested that various oxides of nitrogen are produced by non-equilibrium processes in the atmosphere of Mars, and that these oxides of nitrogen play a major role in the total chemistry of the atmosphere and surface of Mars (Kiess, Karrer, and Kiess, 1960; 1963). In Table 6, we present some calculations of the equilibrium abundance of various compounds in the Martian atmosphere at representative points in Figure 4. Even in the favorable case where oxygen is present as a major constituent, we see that the resulting abundances of the oxides of nitrogen are extraordinarily small. These conclusions are consistent with those of Sagan, Hanst, and Young (1965), who used a much smaller array of equilibrium reactions than are implicitly included here but who considered also photochemical production and breakdown of these oxides. The present results place the equilibrium upper limit on NO_2 several orders of magnitude below the previous calculated values (Sagan, Hanst, and Young, 1964); and below the most recent observational upper limits (Marshall, 1964) by the same factor.

Further conclusions on the nature of the Martian atmosphere in thermodynamic equilibrium could be drawn if reliable estimates were performed of the abundances of such molecules as CO, CH_4, H_2S, SO_3,

O_2. The limited data available are consistent with the existence of thermodynamic equilibrium, but do not demonstrate thermodynamic equilibrium. As in the case of the atmosphere of Venus, the escape of hydrogen, plus the depletion of atmospheric oxygen (here, either by reaction with the crust or by escape from the planetary exosphere) could have led to an evolutionary track in the ternary diagram approximately along the oxidation threshold. The present information is consistent with a small proportion of molecular oxygen in the atmosphere, although the atmosphere could also be slightly reducing. The possibility of a small quantity of organic molecules on the Martian surface depends in part on which side of the oxidation threshold the total atmospheric composition lies. Note from Table 6 that possibly detectable amounts of CH_4 and H_2S are allowed in the reducing case.

7. Jupiter

The observational constraints on the Jovian atmosphere are shown in Table 7. Because there is no way for water to escape from Jupiter, it must be present in significant amounts below the visible clouds. At the clouds it is frozen out because of the low temperatures. We have arbitrarily assumed that the H_2O mixing ratio below the clouds is comparable to that of methane and ammonia. In the clouds it is fixed by the vapor pressure of ice. The thermodynamic equilibrium calculations were carried out for four sets of pressures and temperatures -- in the first case, for a pressure of 1 atm and a temperature of 200° K, corresponding approximately to the region of the clouds (Spinrad and Trafton, 1962; Owen, 1965); and in the second case, for a pressure of 1000 atm and a temperature of 350° K. This point corresponds to the level of the hypothesized water droplet clouds, predicted by Gallet (1963; see also Wildt, Smith, Salpeter, and Cameron, 1963). The concentrations of the major resulting constituents of the Jovian atmosphere at thermodynamic equilibrium are presented in Table 8. The addition of 10^{-6} sulfur, would give the other constituents shown. As first pointed out by Wildt (1937),

the large excess of molecular hydrogen works to greatly reduce the concentration of even simple organic molecules at thermodynamic equilibrium at the lower temperatures. Essentially all carbon is present as methane, all oxygen as water, and all nitrogen as ammonia. The total atmospheric composition gives a point very near the H corner of the ternary diagram. The relative abundance of molecular nitrogen increases fairly rapidly with temperature, but even at 350° K, it is still a very minor atmospheric constituent.

Nevertheless, there is reason to believe that organic molecules may be present in the atmosphere of Jupiter. The bright and contrasting colors of the bands, belts, and spots -- particularly, the Great Red Spot -- surely betoken differences in molecular composition in the vicinity of the Jovian clouds. The turbulent and shifting appearance of the colors means that they are produced in certain regions, transported, and destroyed in other regions. If the colored compounds were produced by a global thermodynamic equilibrium, they would appear to be perfectly uniform. While some small concentration of minerals may be expected due to micrometeoritic infall, it seems unlikely that such materials are differentially distributed over the Jovian clouds; a more reasonable source of chromophores would appear to arise from the major atmospheric constituents, and therefore, be organic materials (see e.g., Urey, 1952; Sagan, 1963). Experiments attempting to simulate the Jovian atmosphere, in which a mixture of the major gases is supplied with energy from a corona discharge, have succeeded in producing such simple organic molecules as HCN, CH_3CN, C_2H_2, C_2H_4, and C_2H_6 (Sagan and Miller, 1960). Their interaction products were predicted to be brightly colored. In experiments relevant to the origin of life on Earth, mixtures of materials which are in effect simulated Jovian environments have been subjected to a wide array of energy sources, and organic molecules have been consistently produced in high yield, provided only that the over-all conditions were reducing (see, e.g., Fox, 1965). Electric discharges and

solar ultraviolet light -- both leading to high electronic temperatures of the excited atoms and both to be expected in the vicinity of the Jovian clouds -- will lead to the production of organic molecules by thermodynamic equilibrium processes.

In a further theoretical test of this contention, we have found that, over a wide range of pressures and temperatures, it is possible to find conditions where polycyclic aromatic compounds are formed in significant quantities for a rapidly quenched system of Jovian composition. In Table 9 are displayed two typical systems: the first, at 1 atm and 1500° K, is intended to represent electrical discharges in the upper (visible) Jovian clouds; the second, at 10^{-6} atm and 1000° K, a hypothetical Jovian thermosphere from which complex organic material rapidly diffuses to lower altitudes. The five most abundant predicted compounds synthesized in the former case are exactly the compounds experimentally produced by corona discharge in the Jovian simulation experiment of Sagan and Miller (1960). In these sample calculations highly colored compounds (such as azulene, asphalt, and azobenzene) are synthesized, as had also been predicted. Thus equilibrium thermodynamics alone tends to produce complex organic compounds--some of them highly colored--provided that an intermittent source of high temperature exists.

8. Acknowledgment

This research was supported in part by NASA Contract No. 21-003-002 with the National Biomedical Research Foundation, 8600 16th Street, Silver Spring, Md., and in part by NASA Grant No. NGR 09-015-023 with the Smithsonian Astrophysical Observatory.

REFERENCES

Allen, C. W. 1963, "Astrophysical Quantitites," second ed. (London: The Athlone Press, 1963).

Baum, W. A., and Code, A. D. 1953, A. J., 58, 108.

Bottema, M., Plummer, W., and Strong, J. 1964, Ap. J., 139, 1021.

Bottema, M., Plummer, W., Strong, J., and Zander, R. 1964, Ap. J. 140, 1640.

Cameron, A. G. W. 1959, Ap. J., 129, 676.

_____. 1963, Lecture notes on Nuclear Astrophysics, Yale University, unpublished.

Chamberlain, J. W. 1962, Appendix 9, in "The Atmospheres of Mars and Venus," ed. W. W. Kellogg and C. Sagan (Washington: National Academy of Sciences -- National Research Council, Publication 944).

_____. 1965, Ap. J., 136, 582.

Chamberlain, J. W., and Hunten, D. M. 1965, Revs. Geophys., 3, 299.

Dayhoff, M. O., Lippincott, E. R., and Eck, R. V. 1964, Science, 146, 1461.

Dollfus, A. 1963, Compt. Rend. 256, 3250.

Eck, R. V., Lippincott, E. R., Dayhoff, M. O., and Pratt, Y. T., 1966 (In preparation).

Fox, S., ed. 1965, "The Origins of Prebiological Systems," (New York: Academic Press).

Gallet, R. M. 1963, private communication.

Hanst, P. L., and Swan, P. R. 1965, Icarus, 4, 353.

Hutchinson, G. E. 1954, "The Biochemistry of the Terrestrial Atmosphere," in The Earth as a Planet, ed. G. P. Kuiper (Chicago: University of Chicago Press) 371.

Kaplan, L. D. 1963, J. Quant. Spectrosc. Radiat. Transfer, 3, 537.

Kaplan, L. D., Münch, G., and Spinrad, H. 1964, Ap. J., 139, 1.

Kiess, C. C., Corliss, C. H., and Kiess, H. K. 1960, Ap. J., 132, 221.

Kiess, C. C., Karrer, S., and Kiess, H. K. 1960, P.A.S.P., 72, 256.

_____. 1963, P.A.S.P., 75, 50.

Kuiper, G. P. 1952, "Planetary Atmospheres and Their Origins," in The Atmospheres of the Earth and Planets, ed. G. P. Kuiper (Chicago: University of Chicago Press) 306.

Marshall, J. V. 1964, Comm. Lunar and Planet. Lab., 2, 167.

Moroz, V. I. 1965, Soviet Astronomy - A. J., 8, 566.

Mueller, R. R. 1964, Icarus, 3, 285.

Owen, T. C. 1965, Ap. J., 141, 444.

Owen, T. C., and Kuiper, G. P. 1964, Comm. Lunar and Planet. Lab., 2, 113.

Pollack, J. B., and Sagan, C. 1965, Icarus, 4, 62.

Sagan, C. 1962, Icarus, 1, 151.

_____. 1963, Proc. XI Internat. Astrophys. Colloq., Liège, 506.

_____. 1966, "Origins of the Atmospheres of the Earth and Planets," in International Dictionary of Geophysics, S. K. Runcorn, ed. (London: Pergamon Press, in press).

Sagan, C., Hanst, P. L., and Young, A. T. 1965, Planet. Space Sci., 13, 73.

Sagan, C., and Kellogg, W. W. 1963, Ann. Rev. Astron. Ap., 1, ed. L. Goldberg, 235.

Sagan, C., and Miller, S. L. 1960, A. J., 65, 499.

Sagan, C., and Pollack, J. B. 1966a, Submitted to J. Geophys. Res.

_____. 1966b. To be published.

Shimizu, M. 1963, Planet. Space Sci., 11, 269.

Spinrad, H. 1962a, P.A.S.P., 74, 156.

_____. 1962b, Icarus, 1, 266.

Spinrad, H., and Richardson, E. H. 1965, Ap. J., 141, 282.

Spinrad, H., and Trafton, L. M. 1962, Icarus, 2, 19.

Studier, M. H., Hayatsu, R., and Anders, E., 1965, Science, 149, 1455.

_____. 1966, In press.

Suess, H. E., and Urey, H. C. 1956, Revs. Mod. Phys., 28, 53.

Urey, H. C. 1952, "The Planets; Their Origin and Development," (New Haven: Yale University Press, 1952).

_____. 1959, Handbuch der Physik, 52, 363.

White, W. B., Johnson, S. M., and Dantzig, G. B., J. Chem. Phys. 28, 751.

Wildt, R. 1937, Ap. J., 86, 321.

_____. 1940, Ap. J., 92, 247.

Wildt, R., Smith, H. J., Salpeter, E. E., and Cameron, A. G. W. 1963, Physics Today, 16, 19.

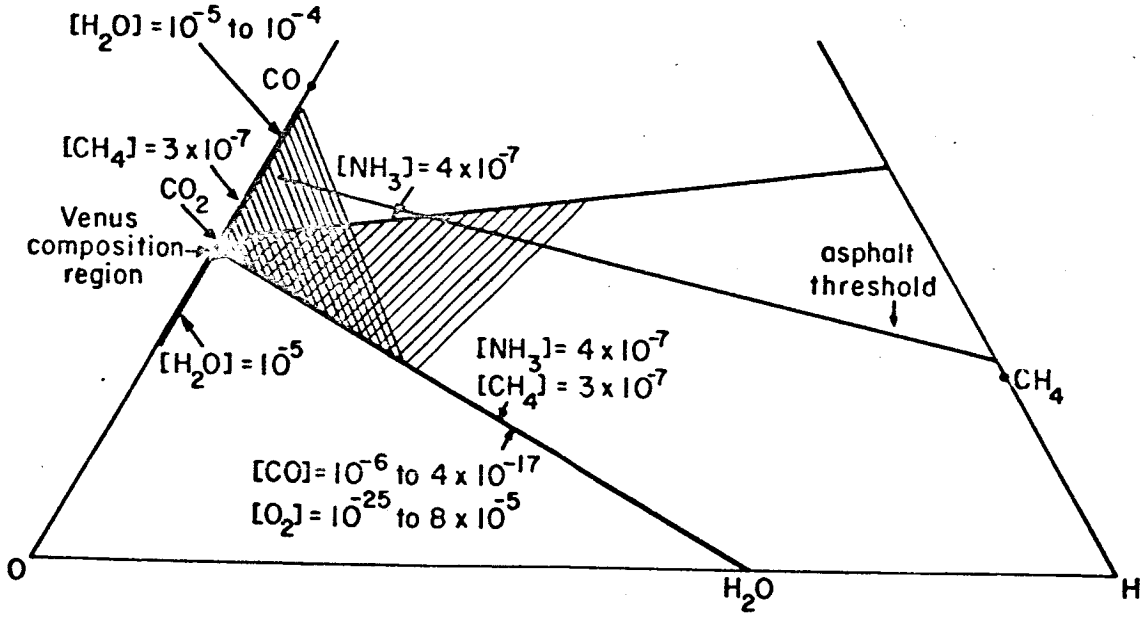

Fig. 1. --C-H-O ternary diagram for the Cytherean atmosphere. The shaded regions are excluded at thermodynamic equilibrium by the observational upper limits on [CH_4] and [NH_3]. For clarity the shading has not been extended through the entire excluded region. The adopted values of [H_2O] and the observed upper limits on [CO] and [O_2] are denoted by lines.

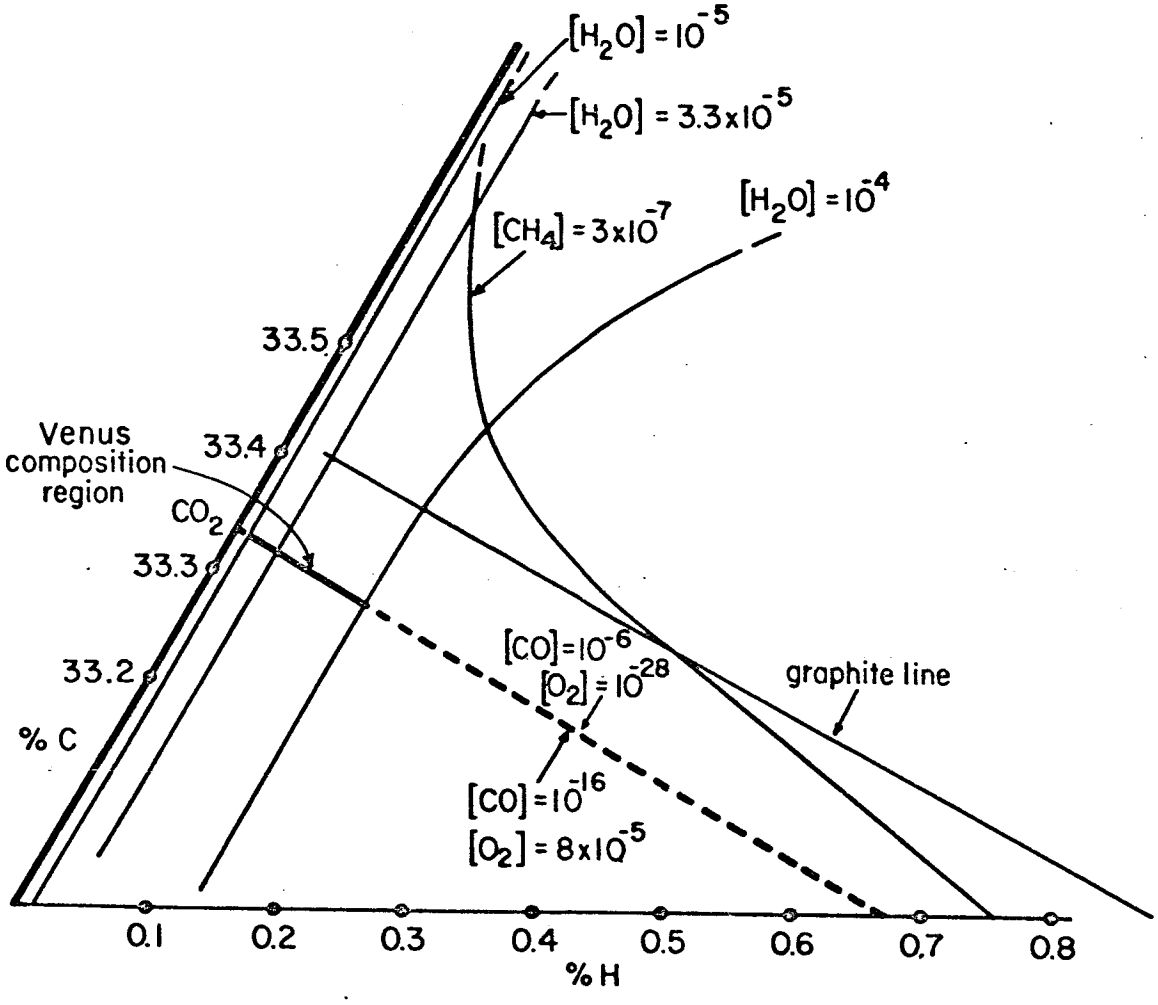

Fig. 2. --C-H-O ternary diagram of Figure 1, here enlarged one hundredfold.

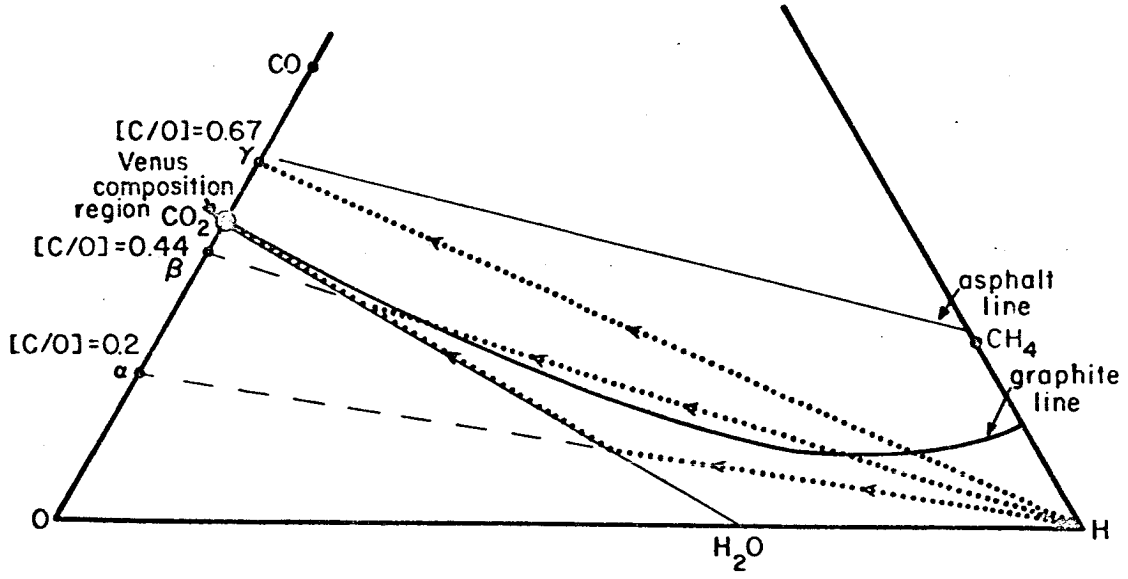

Fig. 3. --Evolution of the atmosphere of Venus. Initial conditions assumed include a large excess of H_2, and three [C/O] abundance ratios. Loss of hydrogen alone causes evolution along the tracks H-α, H-β, and H-γ. Additional loss of oxygen would tend to deflect the lower two evolutionary tracks along the oxidation threshold, the line CO_2 - H_2O. Tracks with initial [C/O] > 0.5 must lose carbon to arrive at the present composition; but the precipitation of graphite or polycyclic aromatics would not lead to the contemporary value of [C/O].

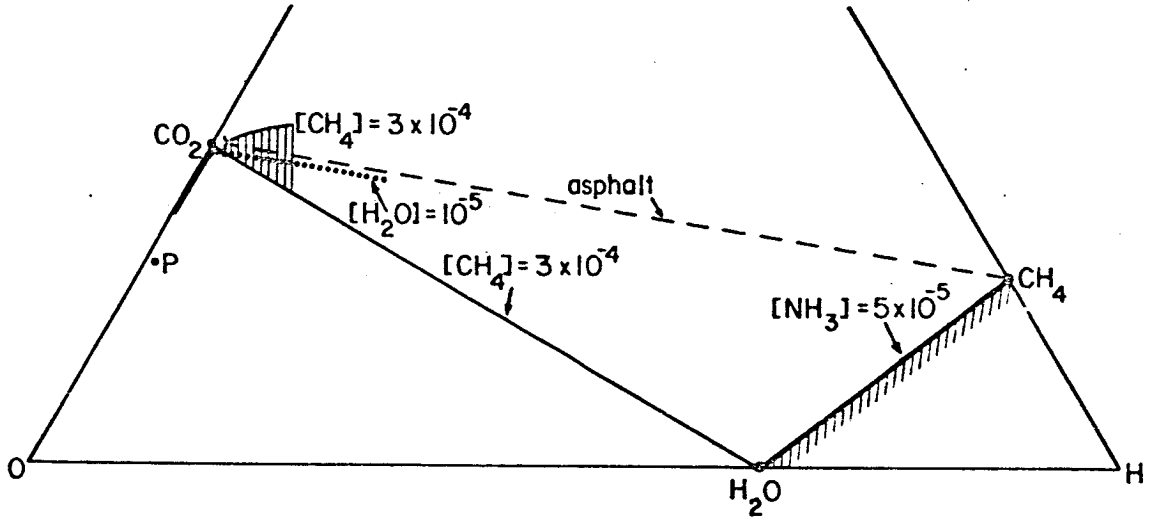

Fig. 4. --C-H-O ternary diagram for the Martian atmosphere. Areas not excluded by observation are localized about the solid portion of the water line, near the CO_2 point. One additional abundance determination can specify the thermodynamic equilibrium composition.

TABLE 1

ADOPTED CHEMICAL COMPOSITION AND PHYSICAL PARAMETERS OF THE TERRESTRIAL ATMOSPHERE (VOLUME MIXING RATIOS ARE DISPLAYED)

O_2	0.2095
O_3	10^{-8} to 10^{-7}
H_2	5×10^{-7}
H_2O	1×10^{-3} to 2.8×10^{-2}
N_2	0.7808
NO_2	5×10^{-10} to 2×10^{-8}
N_2O	5×10^{-7}
NH_3	1.7×10^{-8}
SO_2	1×10^{-6}
CO_2	3.30×10^{-4}
CH_4	1.5×10^{-6}
A	1×10^{-2}
He	5.2×10^{-6}
Ne	1.8×10^{-5}
Pressure	1.0 atm
Temperature	280°K

(References: Allen 1963; Hutchinson 1954)

TABLE 2

THERMODYNAMIC EQUILIBRIUM COMPOSITION OF THE TERRESTRIAL ATMOSPHERE, COMPUTED FROM THE TOTAL ELEMENTAL COMPOSITION OF TABLE 1*

N_2	0.78	H_2S	0
O_2	0.21	CO	0
A	0.01	H_2	0
H_2O	1.0×10^{-3}	CS_2	0
CO_2	3.3×10^{-4}	CH_4	0
SO_3	1×10^{-6}	CH_3SH	0
HNO_3	5×10^{-10}	COS	0
NO_2	7×10^{-11}	Benzene	0
SO_3	3×10^{-17}	Formic acid	0
H_2SO_4	4×10^{-18}	HCN	0
SO_2	8×10^{-20}	NH_3	0
N_2O	2×10^{-20}	Formaldehyde	0
Ozone	6×10^{-32}	Methanol	0

*A mixing ratio of zero is an abbreviation for a value $<10^{-35}$.

TABLE 3

ADOPTED CHEMICAL COMPOSITION OF THE CYTHEREAN ATMOSPHERE (VOLUME MIXING RATIOS ARE DISPLAYED)

O_2	$<8 \times 10^{-5}$
H_2O	1×10^{-6} to 1×10^{-4}
N_2	~0.95
NO_2	$<1 \times 10^{-6}$
N_2O	$<4 \times 10^{-7}$
NH_3	$<4 \times 10^{-7}$
CO_2	$\sim 5 \times 10^{-2}$
CO	$\leq 1 \times 10^{-6}$
CH_4	$<3 \times 10^{-7}$
C_2H_4	$<2 \times 10^{-7}$
C_2H_6	$<1 \times 10^{-7}$
HCHO	$<3 \times 10^{-8}$
Pressure	~50 atm
Temperature	700°K

(References: Kuiper 1952; Spinrad 1962a, 1962b; Spinrad and Richardson 1965; Bottema, Plummer, and Strong 1964; Dollfus 1964; Sagan and Pollack 1966b)

TABLE 4

THERMODYNAMIC EQUILIBRIUM COMPOSITION OF THE CYTHEREAN ATMOSPHERE, COMPUTED FROM TOTAL ELEMENTAL COMPOSITION OF TABLE 2*

Compound	Oxidizing Limit	Reducing Limit
O_2	8×10^{-5}	4×10^{-26}
CO	2×10^{-17}	1×10^{-6}
CO_2	5×10^{-2}	5×10^{-2}
H_2O	1×10^{-5}	1×10^{-5}
N_2	0.95	0.95
H_2	4×10^{-20}	2×10^{-9}
NH_3	4×10^{-30}	4×10^{-14}
HCN	0	2×10^{-18}
NO	7×10^{-9}	2×10^{-19}
NO_2	10^{-9}	4×10^{-31}
N_2O	6×10^{-12}	1×10^{-22}
HNO_3	1×10^{-14}	0
O_3	3×10^{-20}	0
Methane	0	8×10^{-21}
Ethane	0	0
Formic Acid	5×10^{-26}	2×10^{-15}
Formaldehyde	0	3×10^{-19}
Methanol	0	9×10^{-26}
Acetic Acid	0	6×10^{-28}
Methyl Amine	0	6×10^{-33}
Acetylene	0	5×10^{-34}
Benzene	0	0
Asphalt	0	0
SO_2	6×10^{-8}	1×10^{-6}
SO_3	1×10^{-6}	4×10^{-16}
COS	0	1×10^{-7}
H_2S	0	5×10^{-9}
CH_3SH	0	5×10^{-26}
H_2SO_4	5×10^{-17}	2×10^{-26}

*Two extreme systems, $[CO] = 10^{-6}$, $[O_2] = 4 \times 10^{-26}$ and $[CO] = 2 \times 10^{-17}$, $[O_2] = 8 \times 10^{-5}$, are shown. The hypothesized sulfur mixing ratio of 10^{-6} has a negligible effect except on compounds containing sulfur.

TABLE 5

ADOPTED CHEMICAL COMPOSITION OF THE MARTIAN ATMOSPHERE (VOLUME MIXING RATIOS ARE DISPLAYED)

O_3	$<1.3 \times 10^{-6}$
H_2O	$\sim 10^{-5}$
N_2	~ 0.9
NO_2	$<3 \times 10^{-7}$
N_2O	$<5 \times 10^{-3}$
NH_3	$<5 \times 10^{-5}$
SO_2	$<1 \times 10^{-7}$
H_2S	$<2 \times 10^{-4}$
COS	$<5 \times 10^{-5}$
CO_2	$\sim 1 \times 10^{-1}$
CH_4	$<3 \times 10^{-4}$
C_2H_4	$<5 \times 10^{-5}$
C_2H_6	$<3 \times 10^{-5}$
HCHO	$<1 \times 10^{-5}$
Pressure	~ 0.05 atm
Temperature	240°K

(References: Kaplan, Munch, and Spinrad 1964; Owen and Kuiper 1964; Hanst and Swan 1965; Chamberlain and Hunten 1965; Marshall 1965)

TABLE 6

THERMODYNAMIC EQUILIBRIUM COMPOSITION OF THE MARTIAN ATMOSPHERE, COMPUTED FROM THE ELEMENTAL COMPOSITION OF TABLE 5*

Compound	Oxidizing Case	Slightly Reducing Case
N_2	0.82	0.90
CO_2	0.09	0.10
CO	0	3×10^{-13}
O_2	0.09	0
H_2O	1×10^{-5}	1×10^{-5}
CH_4	0	1×10^{-6}
C_2H_6	0	1×10^{-17}
C_6H_6	0	0
H_2	0	1.5×10^{-10}
HCHO	0	5×10^{-29}
HCOOH	0	4×10^{-21}
CH_3	0	2×10^{-18}
CH_3	0	7×10^{-27}
NH_3	0	6×10^{-12}
HNO_3	1×10^{-12}	0
NO_2	6×10^{-13}	0
NO	3×10^{-20}	0
N_2O_4	3×10^{-23}	0
N_2O	1×10^{-23}	0
NO_3	5×10^{-27}	0
N_2O_5	7×10^{-28}	0
N_2O_3	2×10^{-32}	0
HCN	0	2×10^{-29}
SO_3	1×10^{-6}	0
SO_2	5×10^{-22}	5×10^{-28}
COS	0	9×10^{-10}
H_2S	0	1×10^{-6}
$(CH_3)_2SO$	0	3×10^{-12}
CS_2	0	1.4×10^{-18}
CH_3SH	0	6×10^{-19}
H_2SO_4	1×10^{-21}	0

*Two extreme systems, one with $[O_2] = 0$, the other with $[O_2] = 0.09$ -- corresponding to the point P in Figure 4 -- are displayed. The more highly oxidizing conditions favor the presence of oxides of nitrogen, but even then their predicted equilibrium abundances are miniscule.

TABLE 7

ADOPTED CHEMICAL COMPOSITION OF THE JOVIAN ATMOSPHERE (VOLUME MIXING RATIOS ARE DISPLAYED)

	High	Deep
H_2	0.60	0.60
H_2O	$\sim 1 \times 10^{-6}$	$\sim 1 \times 10^{-4}$
NO_2	$< 3 \times 10^{-6}$	$< 3 \times 10^{-6}$
NH_3	2×10^{-4}	2×10^{-4}
CH_4	5×10^{-3}	5×10^{-3}
C_2H_6	$< 1.2 \times 10^{-4}$	$< 1.2 \times 10^{-4}$
CH_3NH_2	$< 3 \times 10^{-4}$	$< 3 \times 10^{-4}$
C_2H_2	$< 6 \times 10^{-5}$	$< 6 \times 10^{-5}$
He	0.36	0.36
Ne	0.03	0.03
Pressure	1 atm	1000 atm
Temperature	200° K	350° K

(References: Kuiper 1952; Spinrad and Trafton 1963; Owen 1965)

TABLE 8

THERMODYNAMIC EQUILIBRIUM COMPOSITION OF THE MAJOR CONSTITUENTS OF THE JOVIAN ATMOSPHERE, COMPUTED FROM THE ELEMENTAL COMPOSITION OF TABLE 7*

	High	Deep
H_2	0.60	0.60
He	0.36	0.36
Ne	0.03	0.03
CH_4	5×10^{-3}	5×10^{-3}
NH_3	2×10^{-4}	2×10^{-4}
H_2O	1×10^{-6}	1×10^{-4}
H_2S	1×10^{-6}	1×10^{-6}
C_2H_6	3×10^{-23}	1×10^{-15}
N_2	6×10^{-22}	1×10^{-16}
CH_3SH	2×10^{-28}	7×10^{-20}
CH_3NH_2	2×10^{-31}	8×10^{-21}
CH_3OH	0	3×10^{-24}
$(CH_3)_2SO$	0	2×10^{-29}
CO_2	0	1×10^{-31}
CO	0	9×10^{-32}
HCHO	0	2×10^{-33}
HCOOH	0	0
HCN	0	0
COS	0	0

*For the sulfur compounds, addition of [S] = 10^{-6} was assumed.

TABLE 9

PREDICTED EQUILIBRIUM IN THE JOVIAN ATMOSPHERE AT HIGH TEMPERATURES AND MODERATE TO LOW PRESSURES

Pressure	~1 atm	$\sim 10^{-6}$ atm
Temperature	1500°K	1000°K
Noble gases	0.4	0.4
H_2	0.6	0.6
CH_4	4×10^{-3}	6×10^{-5}
C_2H_2	2×10^{-4}	2×10^{-3}
C_2H_4	3×10^{-5}	7×10^{-7}
C_2H_6	2×10^{-7}	1×10^{-2}
Benzene	2×10^{-9}	1×10^{-7}
Naphthalene	1×10^{-12}	4×10^{-9}
Asphalt (yellow)	6×10^{-25}	1×10^{-8}
N_2	7×10^{-5}	6×10^{-5}
HCN	6×10^{-5}	9×10^{-5}
NH_3	2×10^{-7}	2×10^{-13}
CH_3CN	6×10^{-8}	2×10^{-10}
Azulene (blue)	5×10^{-14}	2×10^{-9}
Aniline	3×10^{-19}	2×10^{-23}
Azobenzene (red)	3×10^{-28}	3×10^{-33}

The formation of graphite was excluded. High temperatures produced by lightning could permit approach to such equilibria, followed by rapid quenching. Polynuclear aromatics and colored compounds such as azulene tend to form.